Toward Improving the Performance of Highway Bridge Approach Slabs

CFIRE 03-10
September 2011

Authors:
Professor Michael G. Oliva, Gregory Rajek
University of Wisconsin, Madison

Principal Investigator:
Professor Michael G. Oliva
University of Wisconsin, Madison

DISCLAIMER

This research was funded by the National Center for Freight and Infrastructure Research and Education. The contents of this report reflect the views of the authors, who are responsible for the facts and the accuracy of the information presented herein. This document is disseminated under the sponsorship of the Department of Transportation, University Transportation Centers Program, in the interest of information exchange. The U.S. Government assumes no liability for the contents or use thereof. The contents do not necessarily reflect the official views of the National Center for Freight and Infrastructure Research and Education, the University of Wisconsin, the Wisconsin Department of Transportation, or the USDOT's RITA at the time of publication.

The United States Government assumes no liability for its contents or use thereof. This report does not constitute a standard, specification, or regulation.

The United States Government does not endorse products or manufacturers. Trade and manufacturers names appear in this report only because they are considered essential to the object of the document.

Technical Report Documentation Page

1. Report No. CFIRE 03-10	2. Government Accession No.	3. Recipient's Catalog No. **CFDA 20.701**
4. Title and Subtitle **Toward Improving the Performance of Highway Bridge Approach Slabs**		5. Report Date **September 2011**
		6. Performing Organization Code
7. Author/s Professor Michael G. Oliva, Gregory Rajek		8. Performing Organization Report No. CFIRE 03-10
9. Performing Organization Name and Address National Center for Freight and Infrastructure Research and Education (CFIRE) University of Wisconsin-Madison 1415 Engineering Drive, 2205 EH Madison, WI 53706		10. Work Unit No. (TRAIS)
		11. Contract or Grant No. **DTRT06-G-0020**
12. Sponsoring Organization Name and Address Research and Innovative Technology Administration United States Department of Transportation 1200 New Jersey Ave, SE Washington, D.C. 20590		13. Type of Report and Period Covered **Final Report [10/1/2009 to 6/30/2012]**
		14. Sponsoring Agency Code

15. Supplementary Notes
Project completed for the RITA by CFIRE.

16. Abstract

The objective of this study was to quantify the amount of rotation that could develop between an approach slab, after base settlement, and a bridge abutment. A better approach-bridge transition could then be developed by using a ductile concrete to directly connect the approach slab with a bridge deck and lessen or eliminate the annoying "bump" as well as maintenance problems associated with approach slab deterioration. In the future, acceleration bridge construction could then use high quality precast approach slabs directly connected to the bridge with a ductile concrete strip.

To quantify the problems associated with approach slabs, particularly cracking and rotations, an extensive analytical study was conducted. Parameters included in the study were: approach slab length, slab material, subgrade soil type, abutment height, and possible settlement trenches that may develop under the slab near its support on the abutment.

From the analyses it was concluded that end rotation of the approach slab near the abutment varied depending on geometry of the approach slab, trench and abutment as well as with the stiffness of the soil and concrete used in the analyses. A maximum rotation of 0.0045 radians was computed from the analyses in a situation with a loose soil and a 4 ksi concrete approach slab but 0.002 radians could be used for normal design.

17. Key Words bridge approach slabs, highway bridges, approaches, ductile concrete, precast paving	18. Distribution Statement **No restrictions. This report is available through the Transportation Research Information Services of the National Transportation Library.**		
19. Security Classification (of this report) **Unclassified**	20. Security Classification (of this page) **Unclassified**	21. No. Of Pages 82	22. Price **-0-**

Form DOT F 1700.7 (8-72)   **Reproduction of form and completed page is authorized.**

TOWARD IMPROVING THE PERFORMANCE OF HIGHWAY BRIDGE APPROACH SLABS

EXECUTIVE SUMMARY

Since the primary purpose of a bridge approach slab is to create a smooth transition from the roadway to the bridge, a "bump" experienced by roadway users on entering or exiting a bridge is evidence of failure of an approach. The failure is likely due to differential settlement. Differential settlement occurs when one end of the approach slab (the end supported by the roadway base) settles a different amount than the other end (supported by a bridge abutment). This is a pervasive condition since 25% of all bridges in the United States have problems associated with their approach slabs.

The objective of this study was to quantify the amount of rotation that could develop between an approach slab, after base settlement, and a bridge abutment. A better approach-bridge transition could then be developed by using a ductile concrete to directly connect the approach slab with a bridge deck and lessen or eliminate the annoying "bump" as well as maintenance problems associated with approach slab deterioration. In the future, accelerated bridge construction could then use high quality precast approach slabs directly connected to the bridge with a ductile concrete strip.

To quantify the problems, particularly cracking and rotations, associated with approach slabs an extensive analytical study was conducted at the University of Wisconsin, Madison. Finite element analysis of the approach slab and bridge were run with various parameters under service loading. These included approach slab length, slab material, subgrade soil type, abutment height, and possible settlement trenches that may develop under the slab near its support on the abutment.

From the analyses it was concluded that end rotation of the approach slab near the abutment varied depending on geometry of the approach slab, trench and abutment as well as with the stiffness of the soil and concrete used in the analyses. A maximum rotation of 0.0045 radians was computed from the analyses in a situation with a loose soil and a 4 ksi concrete approach slab. The majority of the rotations in other cases were below 0.002 radians. For normal soil conditions the expansion joint or ductile concrete between the approach slab and abutment should be designed to accommodate a minimum of 0.002 radians of rotation.

The susceptibility of the approach slab to cracking was influenced by the height of the abutment, trench length, slab length, soil stiffness, and concrete stiffness. Taller abutments increase the likelihood of concrete cracking in the approach slab. This was particularly true for all settlement trenches with length less than 6ft. When the settlement trench was 6ft or more in length the slab behavior was not particularly sensitive to abutment height.

The length of the approach slab has little effect on the likelihood of cracking or amount of end rotation for slabs greater than 10ft in length.

Stiff soil under the approach slab reduced the probability of concrete cracking. The risk of concrete cracking increased as the soil stiffness decreased. With loose soil, slab cracking can be expected with normal strength (4ksi) concrete. Cracking was less likely when a concrete with a higher compressive stress was used for the approach slab (i.e. 8ksi vs. 4ksi).

Table of Contents

1. Introduction: Approach Slab "Bumps"

Problem and Background

Highway bridge approach slab settlement and deterioration has been studied by various researchers throughout the past 20 years. Specifically, researchers have studied differential settlement in approach slabs, as this has been cited as the main cause for failure of approach slabs (Seo, 2003).

Since the primary purpose of the approach slab is to create a smooth transition from the roadway to the bridge, failure of an approach slab is evidenced by a "bump" experienced by roadway users when they enter or exit a bridge. Differential settlement occurs when one end of the approach slab (typically supported by soil) settles a different amount than the other end (typically supported by a bridge abutment). Previous research attributes some causes of differential settlement to consolidation of backfill materials, poor drainage, poor construction methods (Seo, 2003), expansion joint failure, and the type of abutment (Helwany, et al., 2007).

Once differential settlement reaches a depth of ½'', roadway users are able to distinguish a "bump" at the time of the bridge exit / entry (Wahls, 1990). Differential settlement of 1" becomes problematic to the Department of Transportation (DOT), as repair or replacement of the approach slab is recommended at this depth (Zaman, et al., 1991); serious rider discomfort is experienced when a differential settlement of 2" or more exists (Stark, et al., 1995).

Several DOTs have noted the formation of a void space beneath problematic approach slabs. Research performed on loose backfill discovered the maximum geometry of the void was dependent on abutment geometry (Cosgrove, et al., 2003).

In order to assess the range of approach slab failure rates across multiple States, a survey was sent to various state DOTs to assess the problems associated with expansion joint failures occurring between the approach slab and bridge in their region. Thirteen of the eighteen DOT respondents utilized expansion joints between the approach slab and bridge: of

the DOTs that use expansion joints, 12 had reported expansion joint failures (CTC & Associates, LLC, 2010).

This report will focus on the overall problem of highway bridge approach slab failure and effects of loading on approach slab durability and performance.

Objectives

The main objective of this research was to determine an allowable range of end rotation for the approach slab at the abutment-approach slab interface and means of accommodating that deformation. Secondary objectives were to:

- Determine which variables influence approach slab cracking;
- Determine a LL impact factor that would define the load causing approach slab cracking, as a multiple of the service load, for each case considered;
- Identify variables that have the largest impact on approach slab end rotation.

Scope

This investigation focused on the end rotational behavior of approach slabs as well as approach slab cracking and methods of accommodating that rotation at the joint with the bridge.

The first step involved prediction of the possible rotation that could occur in approach slabs when one end supported on roadway fill settled. Parametric studies that varied the geometry of the settlement trench, abutment height, approach slab length, soil stiffness, concrete stiffness, and joint restrictions placed between the roadway and approach slab were varied to determine their effect on the behavior of the approach slab. These investigations were limited to:

- Loading
  - The live load (LL) considered consisted of one AASHTO HL93 (AASHTO 2010) tandem design truck without lane loading. The

tandem created a loading that was more detrimental than the design truck.

- o No dynamic or cyclic loading was considered.
- o Pile base and pile-abutment connections were considered to be rigid.
- Geometry
  - o Only non-skewed approach slabs were examined.
  - o The effects were measured using a single lane.
  - o Only non-integral abutments were considered.
- Concrete Properties
  - o Elastic properties were used for all concrete components.
  - o A single value for Poisson's ratio was assumed..
  - o A cracked moment of inertia was used in areas of the approach slab that developed strains exceeding the cracking strain as defined by ACI (ACI 318, 2008).
  - o Volume changes from shrinkage, creep, and thermal variation were not considered.
- Soil
  - o A soil sensitivity study was performed to verify the upper and lower bounds of the soil properties.
  - o The natural soil types at a given location were not considered.
  - o The location of the water table was not considered.
  - o Volume changes from creep and thermal changes in the soil were not considered.

2. Literature Review

Problems Associated with Highway Bridge Approach Slabs

Highway bridge approach slabs are intended to create a smooth transition between the roadway and bridge. Differential settlement often occurs between the bridge and roadway facilitating the need for special approach slabs (Ha, et al., 2002). An expansion joint is typically placed between the approach slab and abutment to accommodate volumetric changes in the approach slab and bridge, accommodating rotations that develop at the end of the approach slab, as well as preventing surface water from infiltrating through the joint and into the fill beneath the approach slab causing erosion.

Problems associated with bridge approach slabs have been investigated by a large number of researchers and transportation officials. On average, 25% of all bridges in the United States have problems associated with approach slabs (Seo, 2003). The most noticeable problem that users experience is the bump that is created by differential settlement between the approach slab and the firmly based bridge. Previous research has identified the settlement of the embankment supporting the approach due to a weak natural soil, slow compression of the embankment fill, voids under the pavement due to erosion, abutment displacement due to pavement growth, slope instability, and temperature cycles (Seo, 2003) as the main reasons for the formation of the bump. The same study noted the bump became more severe if a high embankment, an abutment constructed on piles, high average daily traffic, soft natural soil, intense rain storms, extreme temperature cycles, and steep approach gradients existed. Conclusions gathered from a Federal Highway Administration (FHWA, 1990) study attribute some approach slab deterioration problems to:

1. Movement of the natural soil under the embankment due to expansive soils, frost heave, or settlement,
2. Construction practices that fail to meet design requirements,
3. Inadequate or poor quality fill,
4. Vehicular overloading or inadequate designs resulting in excessive deflection,
5. Inadequate or poor drainage,

6. Loss of underlying fill due to erosion,

7. Inadequate or poor joints between the approach slab and bridge deck, and

8. Thermal expansion and contraction of the approach slab.

The problems outlined above can be summarized under four categories (Helwany, et al., 2007):

1. Poor pavement performance,

2. Abutment type,

3. Soil deformation, and

4. Poor drainage.

Previous research performed by Wahls (1990), Zaman (1991), Stark (1995), Ha (2002), Seo (2002), White (2007), and Helwany (2007) identified many of the problems associated with highway bridge approach slabs and methods to mitigate those problems. Figure 2.1 summarizes some of the most common problems encountered at bridge sites by White et al. (2007).
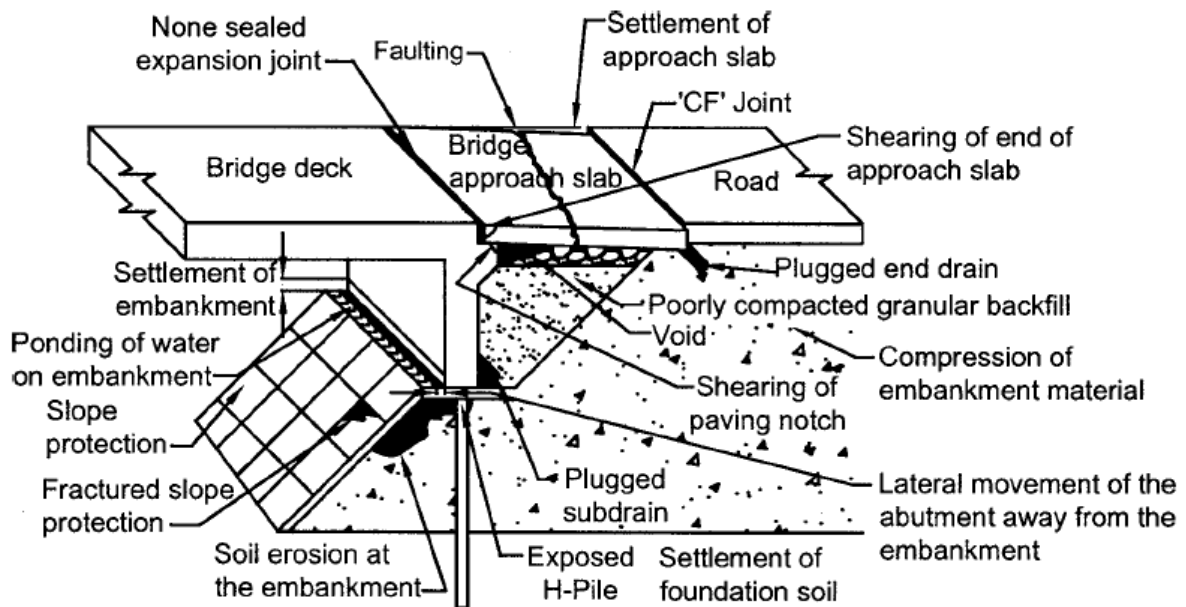

Figure 2.1 – Common problems encountered at bridge sites.

Pavement Performance

Poor performance of the pavement may be caused by changes in temperature, improper reinforcement, joint deterioration, and/or actual loads exceeding the design load of the pavement (Helwany, et al., 2007).

Precast approach slabs have been implemented in Iowa in an attempt to improve the performance of the approach slab. Pre-tensioning and post-tensioning were utilized in the construction of the approach slab as a means of controlling cracking and improving the durability of the slab. Those approach slabs were designed to 'span' a maximum 6.1 foot void in the sub-grade (Merritt, et al., 2007). The long term behavior of this precast approach slab construction method has not been identified yet.

Abutment Type

Previous research has found that the behavior of the approach slab is influenced by the geometry and type of abutment used for the bridge. The performance of the approach slab and bridge was categorized as structurally affected when the lateral deflection exceeds 2" and/or the vertical deflection exceeds 4" (Wahls, 1990).

The Wisconsin Department of Transportation (WisDOT) identifies three main abutment types as closed, stub/sill, and spill-through (Wisconsin Department of Transportation, 2009). These abutments are constructed on both deep and shallow foundations. Only abutments on deep foundations were considered in this research.

Closed type abutments are designed to retain the full lateral soil pressure created from backfill over the entire height of the embankment. For this reason, the closed type abutments are commonly known as full height abutments. Figure 2.2 displays a closed type abutment.
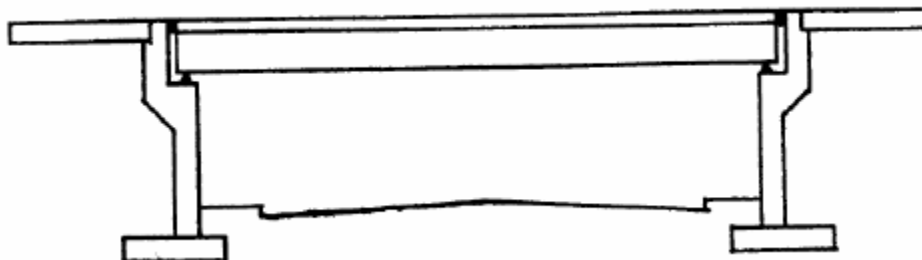
Figure 2.2 – Closed abutment (Helwany et. al, 2007).

Stub/sill type abutments are designed to resist a portion of the soil pressure created from the embankment. These abutments are commonly called partial height abutments and generally utilize a slope to retain the embankment. Figure 2.3 displays a stub/sill type abutment.
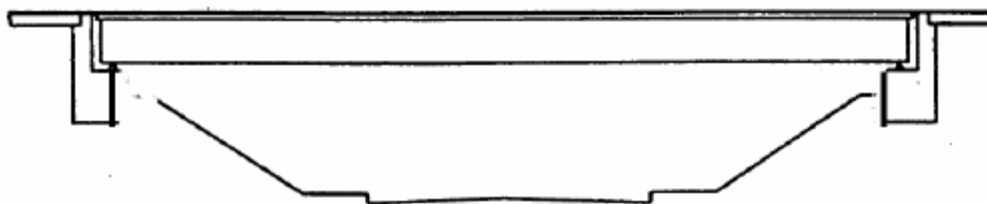
Figure 2.3 – Stud/sill abutment (Helwany et. al, 2007).

Spill-through abutment types are initially designed to be stand-alone abutments as well as having some capacity to resist soil pressure. They are commonly used in locations where future expansion would remove the embankment. These abutment types are designed to act as piers when the embankment is removed. Spill-through abutments are not used by WisDOT. Figure 2.4 displays a typical spill-through type abutment.

Figure 2.4 – Spill-through abutment (Helwany et. al, 2007)

Soil Deformation

Deformation of the underlying soil has a negative impact on the behavior of the approach slab. The water content of the soil near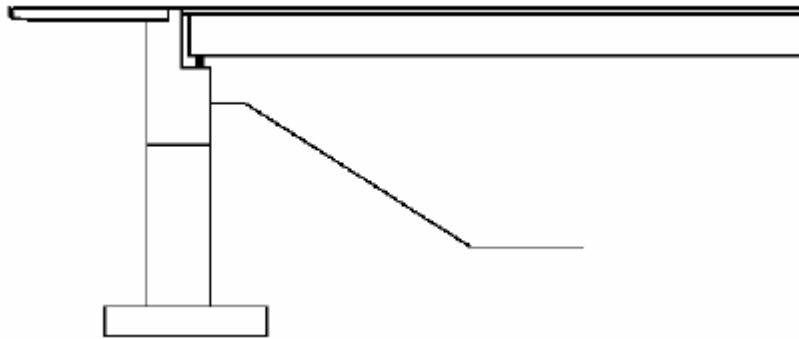 the abutment is often higher than soil located a distance away from the abutment. This increase in water content results in lower strength leading to a higher compressibility of natural cohesive soils (Seo, 2003).

Helwany et al. identified multiple construction problems encountered during the compaction of the fill under the approach slab. These problems include:

- Lifts that are too thick resulting in poor compaction.
- The use of improper compaction equipment.
- Limited access near the abutment for compaction equipment.
- Compacting outside of the optimum moisture content.
- Lack of inspection or testing of the relative density of the soil.
- The use of cohesive soils.

The effects of cyclic loading on loose sand placed near integral abutments that utilized an approach slab were studied by Cosgrove and Lehane (2003). Multiple tests were performed that simulated active and passive conditions. In the tests large volumetric changes in the soil near the abutment were observed (Cosgrove, et al., 2003). Approach slab settlement reached the maximum at a horizontal distance of 75% of the total embedment depth. Figure 2.5 displays the normalized surface settlement with respect to abutment height.

Their study concluded that the geometry of the settlement trench was dependent on abutment height.
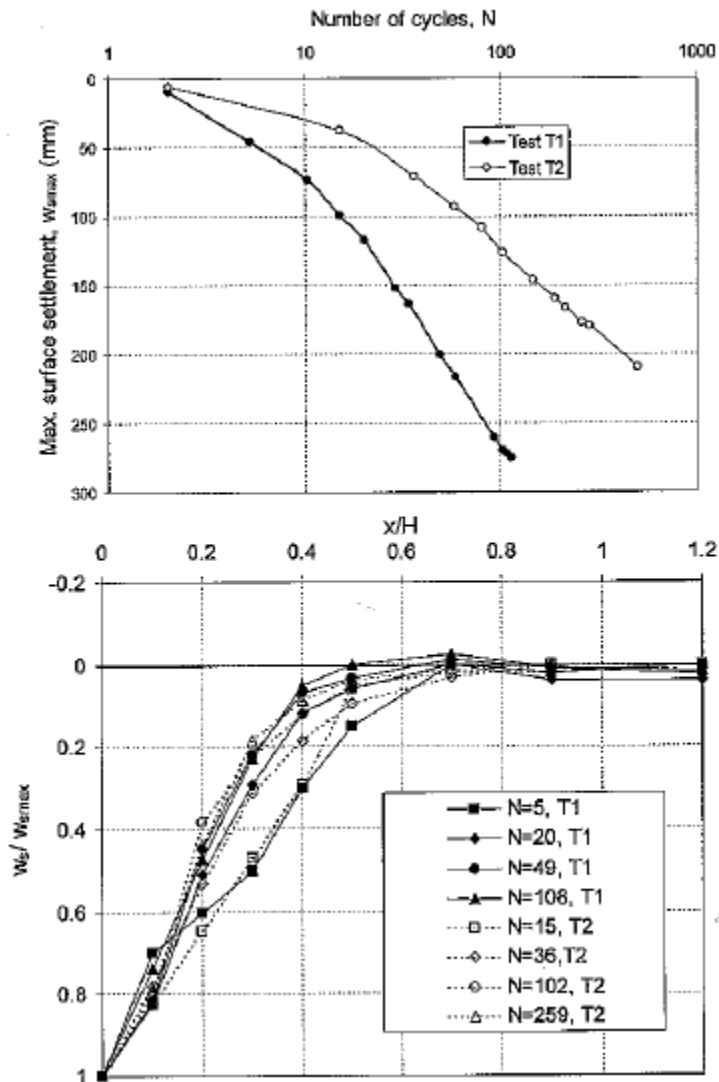

Figure 2.5 – Variation with number of cycles of the maximum settlment(w_{smax}) and the normalized surface settlement profile. H is the abutment height and x is distance from abutment. (plots from Cosgrove, et al., 2003).

Drainage

   Improper drainage leads to erosion and weakening of the fill beneath approach slabs. Typical devices used for drainage include plastic drainpipes, weep holes in the abutment, and geosynthetic materials (Hoppe, 1999). When these devices fail, water infiltrates the underlying fill. Water can also invade the fill from weak/dysfunctional expansion joints or cracks in the approach slab (Puppala, et al., 2008). This water can cause erosion of the fines facilitating the creation of a void space beneath the approach slab, usually adjacent to the abutment where the joint is located.

3. Numerical Modeling

Introduction

The finite element analysis program, Abaqus, was used for the numerical analysis of the behavior of bridge approach slabs. Components considered in the model included the roadway, approach slab, abutment, fill, bridge, and live load truck. Figure 3.1 identifies these components.
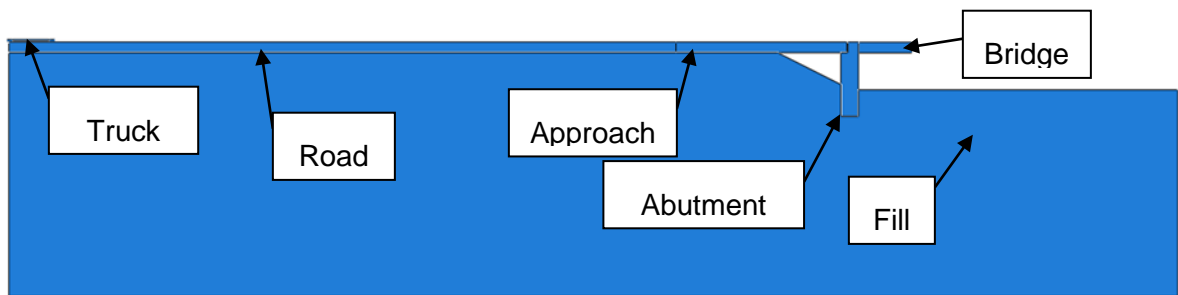
Figure 3.1 – Components considered in numerical model.

Initial Models – Development of Modeling Scheme

Initial models that were created had simplified, but inaccurate boundary conditions imposed on the approach slab. The approach slab was connected to the abutment with a shear coupling (horizontal and vertical displacement of the approach slab relative to the abutment was restricted) at the bottom edge of the approach slab. Another shear coupling connected the roadway to the approach slab. This coupling was placed at the top of the roadway-approach slab joint. Figure 3.2 displays the initial model and location of each shear coupling. Both couplings allowed excessive approach slab end rotation. Figure 3.3 displays a scaled picture of the deformed approach slab.
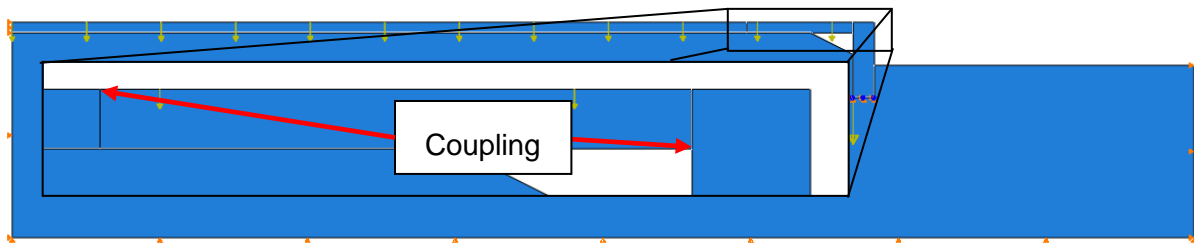
Figure 3.2 – Approach slab restraints placed on initial model.
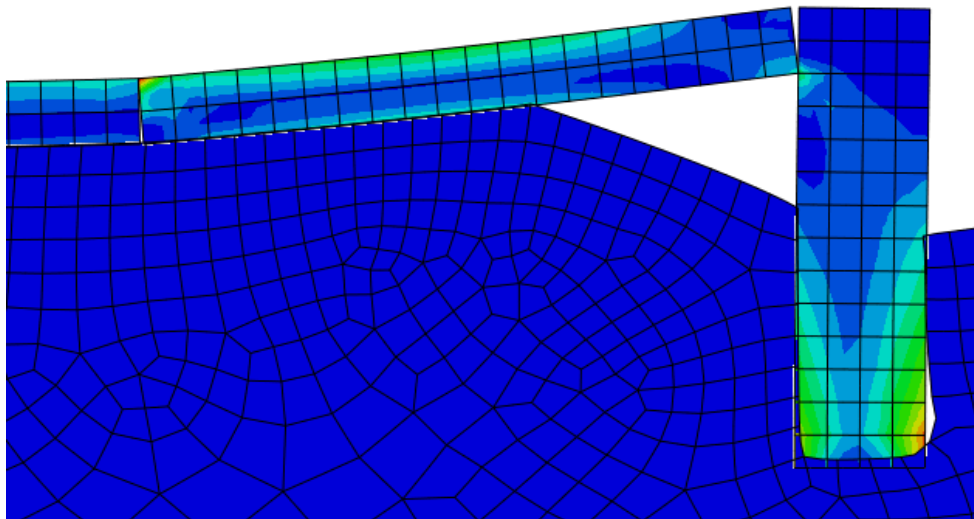
Figure 3.3 – Deformed approach slab calculated in initial model.

The model was modified to better accommodate construction practices. The location of the coupling between the roadway and approach slab was moved to the quarter point to simulate the effect of dowel bars. Abutment geometry was altered to allow the approach slab to be supported by a paving notch. The paving notch allowed the shear coupling between the approach slab and abutment to be removed from the analysis.

Loading was the second major flaw with the initial model. The initial loading scheme applied axle loadings for a standard HL93 AASHTO truck (shown in Figure 3.4) to the roadway and approach slab at seven foot intervals.
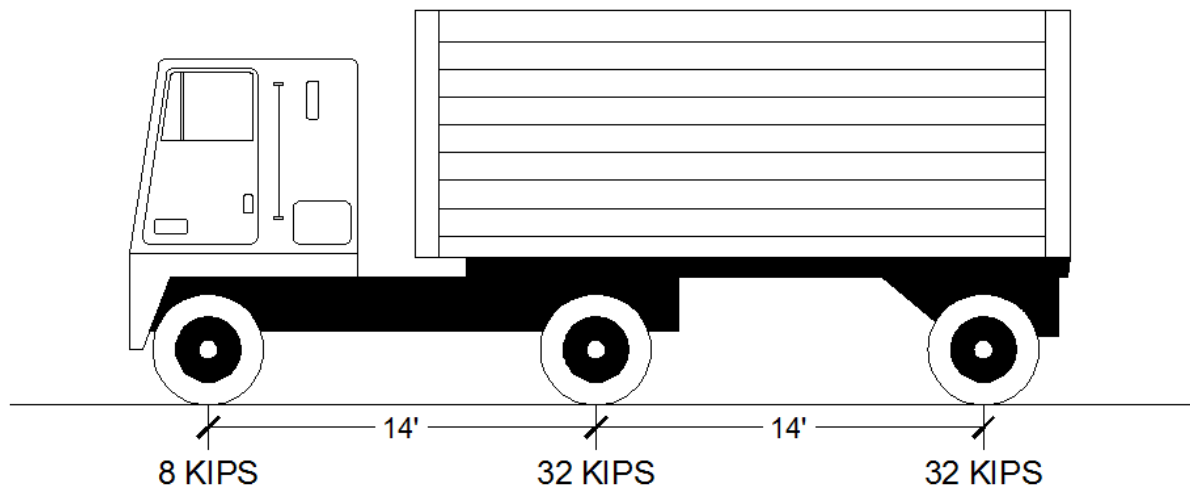
Figure 3.4 – HL93 standard design truck.

The truck axle loads were applied at two locations along the approach slab. These locations are shown in Figure 3.5. This loading scheme failed to apply the axle load(s) at the critical location of the approach slab.
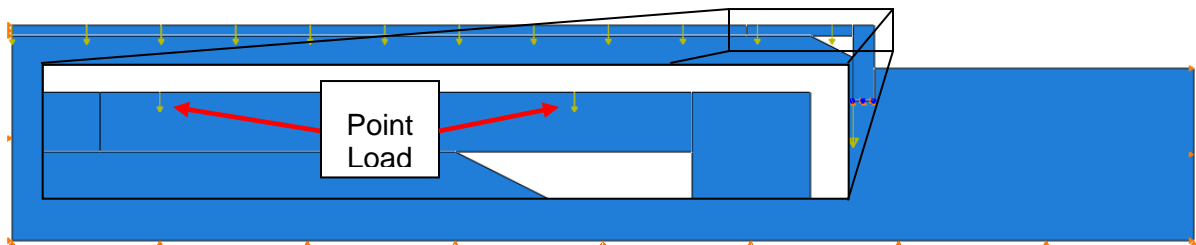
Figure 3.5 – Approach slab point loads used in initial model.

The initial model considered the axle load and spacing of the AASHTO HL93 standard truck alone. The axle loads and spacing of the AASHTO HL93 standard truck were subsequently compared to the AASHTO HL93 tandem truck, shown in Figure 3.6, over the short span (the maximum approach slab considered in this work) to determine which truck produced the largest moments.
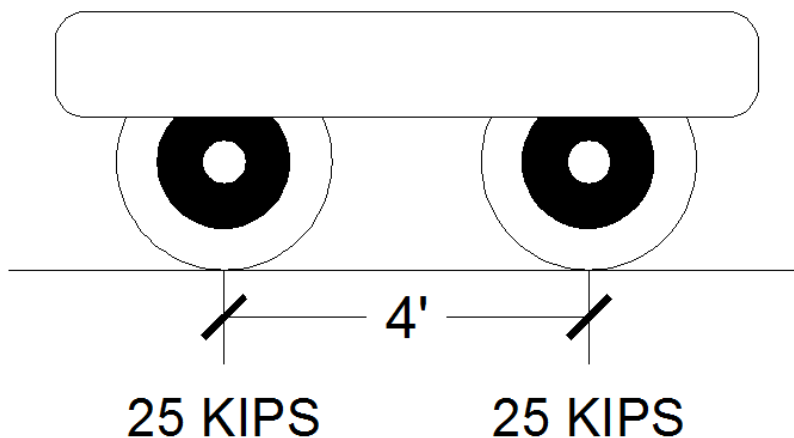
Figure 3.6– HL93 tandem design truck.

The maximum moment induced in the approach slab was calculated for multiple approach span lengths using axle loads and spacings from each design vehicle. Figure 3.7 displays the maximum moment vs. span length created by each truck.

Figure 3.7– HL93 design truck moments.

The moment created by the standard truck would control for spans shorter than 11'. Moments created from the HL93 tandem truck control for spans between 12' and 20'. The shortest approach slab considered in this work was 10'. The HL93 tandem truck was used for the analyses conducted on models with a 10' approach slabs since the error, as compared to truck moments, was only 6% difference in maximum moment.

Soil Sensitivity Study

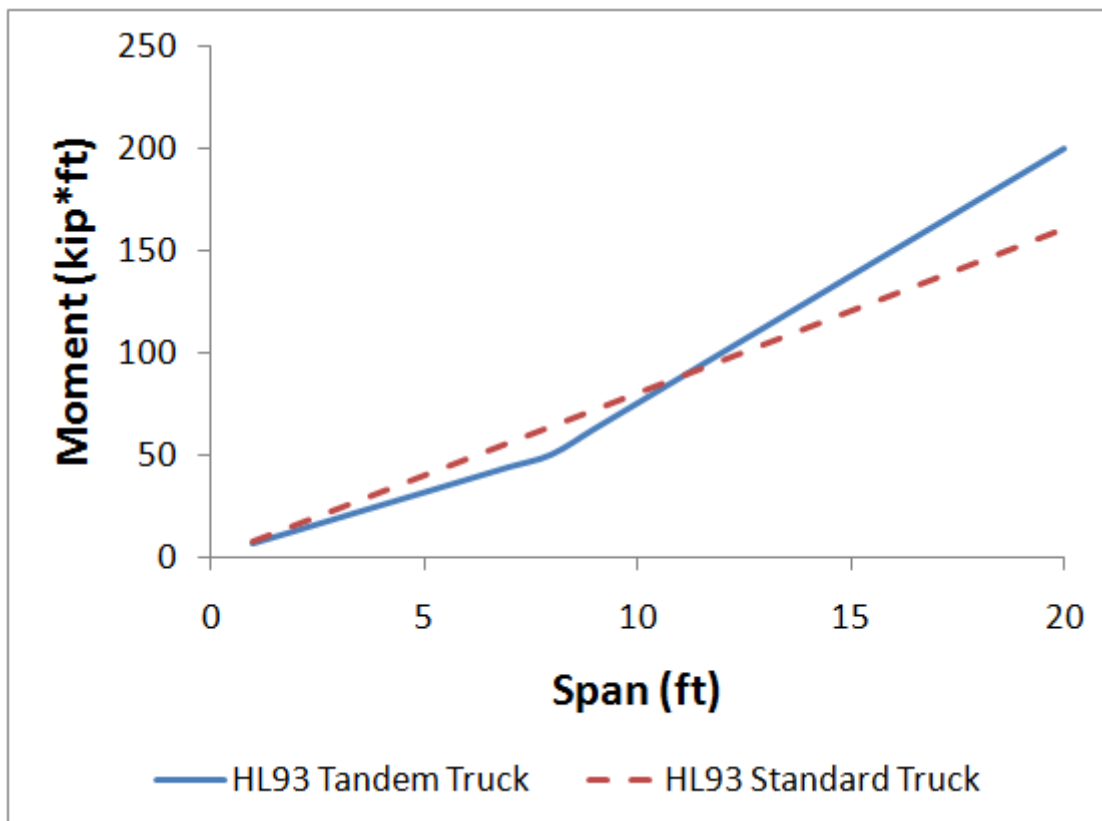*Introduction:* A sensitivity study was performed on the initial model to determine how sensitive approach slab deflections were with respect to soil stiffness and what range of soil stiffnesses should be examined later in detail. All analyses conducted for this study utilized the same constraints that were identified in the initial model. A control point on the approach slab was designated to be used for the comparison between each analysis performed in the sensitivity study. The model used for the soil sensitivity is shown in Figure 3.8.
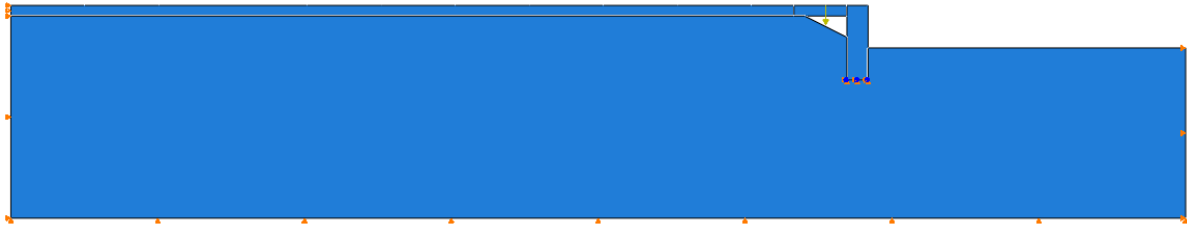
Figure 3.8– Soil sensitivity model.

Soil Properties: The stiffness of the soil was varied to determine how sensitive the model was to changes in soil stiffness. The lower bound of the model utilized a shear modulus (G) of the soil, calculated using Equation 3.1 (assumes soil is isotropic), of 1.45 ksi.

$$G = \frac{E}{2*(1+\upsilon)} \hspace{3cm} (3.1)$$

Where:	G	=	Shear modulus (ksi)
	E	=	Modulus of elasticity (ksi)
	ν	=	Poisson's ratio

The shear modulus of the soil was increased by a factor of two for each subsequent analysis. This was continued until the shear modulus of the soil reached 558 ksi, the upper bound of the soil considered in this study.

Loading and Boundary Conditions: Boundary conditions placed on the sensitivity study models were consistent with the boundary conditions prescribed in the initial model. A 1 kip point load placed at the top of the approach slab over the middle of the settlement trench was the only load placed on the structure, apart from gravity loading. Displacement of the node at the bottom of the approach slab directly under the applied load was used as the control point for the comparison between the differing models.   Figure 3.9 displays the location of the point load and control point used for each analysis.
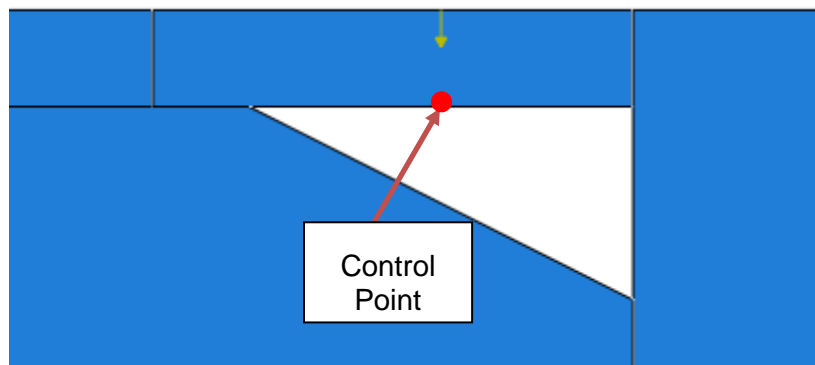
Figure 3.9– Control point used for soil sensitivity study.

Soil Sensitivity Results: Deflection of the specified point was plotted against the shear modulus of the soil to determine how sensitive the behavior of the approach slab was to soil stiffness. Table 3.1 lists the soil stiffness and corresponding deflection determined from each analysis.

E (ksi)	G (ksi)	Δ (in)
1.45	0.56	9.03E-04
3.92	1.51	5.48E-04
7.83	3.01	3.44E-04
15.7	6.02	2.07E-04
31.3	12.0	1.26E-04
61.4	23.6	8.13E-05
125	48.2	5.67E-05
251	96.4	4.27E-05
501	193	3.40E-05
1003	386	2.82E-05
1450	558	1.25E-05

Table 3.1 – Soil sensitivity study results.

Figure 3.10 displays a plot of the control point deflection with respect to soil stiffness.
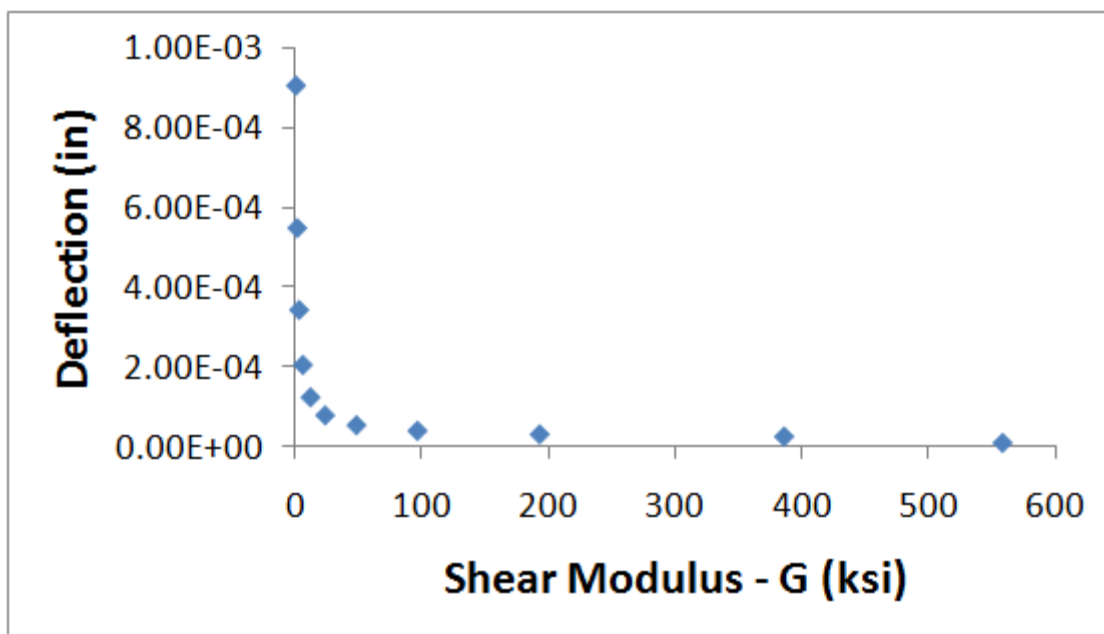
Figure 3.10– Deflection vs. soil stiffness sensitivity study plot.

Soil Sensitivity Discussion: The sensitivity of the approach slab to soil stiffness graphically mimics the behavior of an exponentially decaying function. Soils with a shear modulus greater than 6.02 ksi (41.5 MPa) had little effect on the approach slab deflections.

Soils with a shear modulus less than 6.02 ksi had a large impact on the behavior of the approach slab.

The slope between points on Figure 3.10 were used to quantitatively define the point at which the soil begins to have a substantial effect on the behavior of the approach slab. The maximum slope considered to be influential for this study was -0.00005. Figure 3.11 displays the slope of each line segment used to determine when the stiffness of the soil has a significant impact on the behavior of the approach slab.
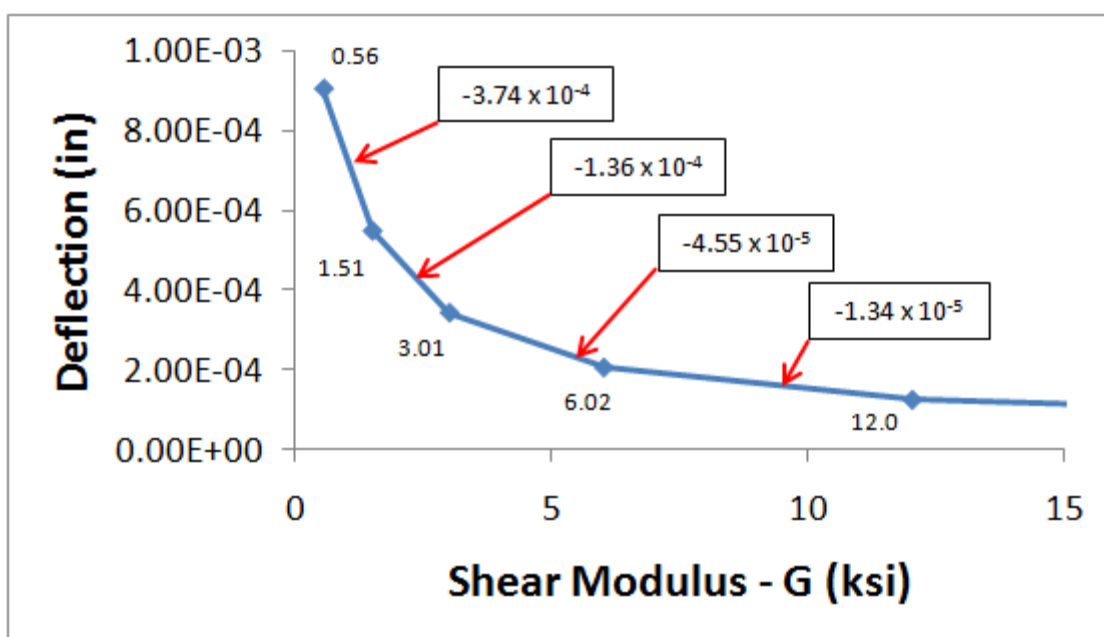
Figure 3.11 Slopes of line segments between points calculated from soil sensitivity study.

The stiff soil bound was reaffirmed as a result of the soil sensitivity study. The stiff soil bound used in subsequent analyses had a shear modulus approximately equal to 5.60 ksi.

Validation - Approach Slab Modelling/Deformation

Introduction: A validation was performed to verify the behavior of the truck and approach slab in Abaqus. The verification model was void of soil and utilized gravity and HL93 tandem truck axle loads to generate deflection of the approach slab. The deflection of the approach slab as determined from the analysis was compared to a theoretical beam with similar loading and boundary conditions. Figure 3.12 displays the model used for validation.

Figure 3.12– Model used for approach slab deflection verification.

Loading and Boundary Conditions: Unique boundary conditions were utilized on the model due to the absence of soil. Displacement based boundary conditions were placed along the bottom of the roadway, abutment, and bridge (but not approach slab) to restrict horizontal and vertical displacement. Rotational displacement of the bottom of the abutment was restrained in addition to boundary conditions previously mentioned. This fixed restraint simulated a rigid pile and pile connection at the base of the abutment.

Interaction between the approach slab and roadway was controlled by a shear coupling placed at a distance of $t/4$ from the top of the approach slab with t being the approach slab thickness. Figure 3.13 displays the location of the coupling.
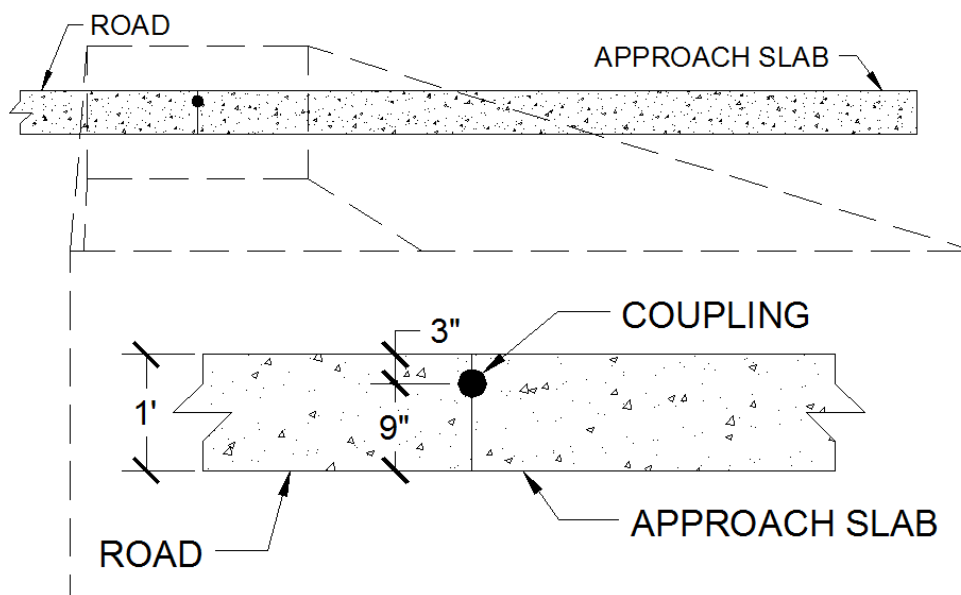
Figure 3.13 – Coupling location used in model verification.

A thickness (*t*) of 12" was used for the thickness of the approach slab and roadway. The location and restraints placed on the shear coupling acted as a fixed support for the approach slab. This was due to the formation of a couple as shown in Figure 3.14.
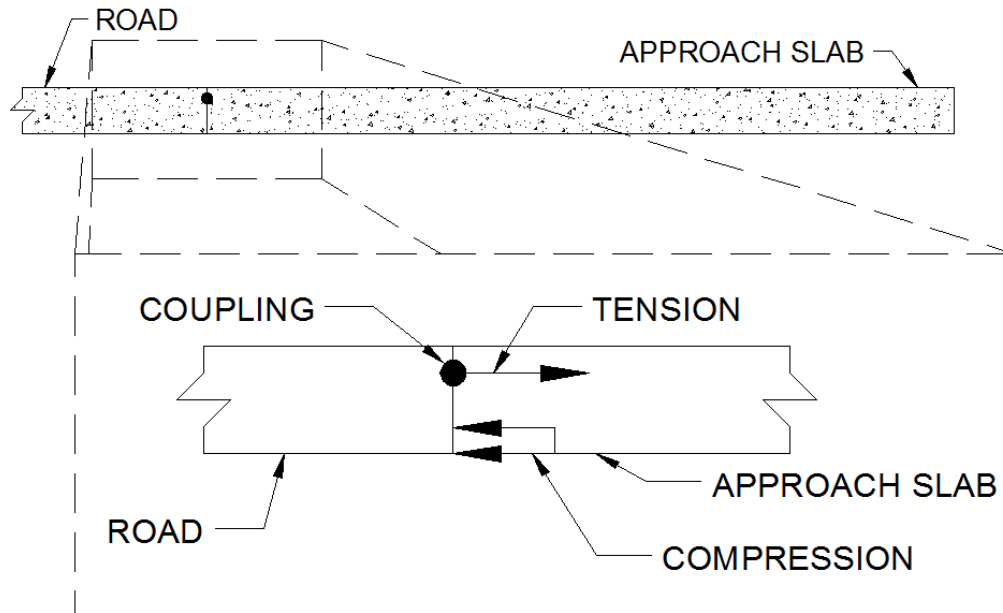
Figure 3.14 – Roadway-approach slab support.

The contact between the approach slab and abutment was controlled by a frictionless surface-to-surface contact constraint. The frictionless contact allowed the paving notch to behave like a roller during the analysis.

Gravity and HL93 tandem truck axle loads were used in the analysis. The design vehicle was placed on the left side of the roadway, as depicted in Figure 3.15, while gravity was applied to the model. After gravity and the axle loads were applied, the truck was moved towards the approach slab in step-by-step increments less than or equal to 4 inches until both axles had traveled the full length of the approach slab. Figure 3.16 shows the final position of the truck after the analysis.
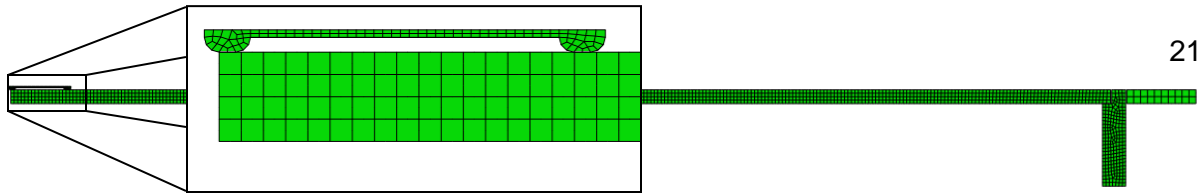
Figure 3.15 – Initial position of the HL93 tandem design truck.
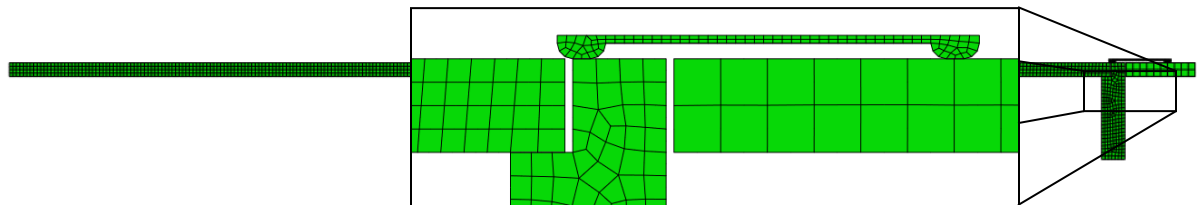
Figure 3.16 – Final position of the HL93 tandem design truck.

        Approach Slab Deformation Results and Discussion: Deflection of the approach slab determined from the analysis was compared to the theoretical deflection of a beam with similar loading and boundary conditions. The deflection of the approach slab was compared to the theoretical beam when the left axle of the tandem had traveled 7'-1 1/8" along the approach slab. Figure 3.17 displays the position of the tandem and theoretical beam used in the validation.
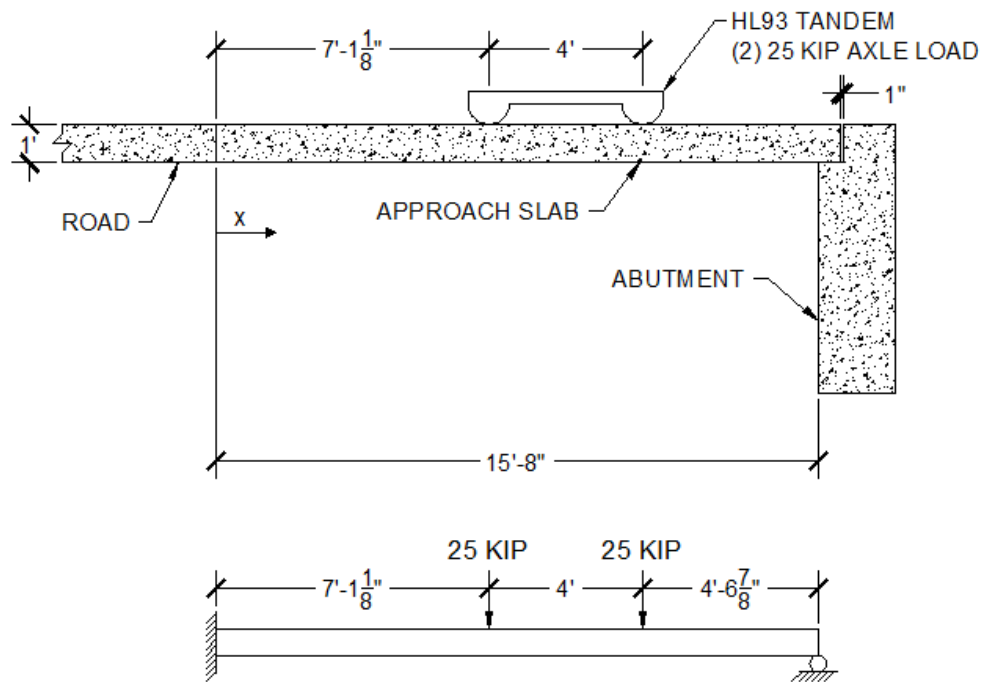
Figure 3.17 – Position of tandem and theoretical beam used for model validation.

Superposition was used to determine theoretical deflection of the beam. Figure 3.18 compares the deflection calculated from the finite element analysis and the theoretical beam deflection.
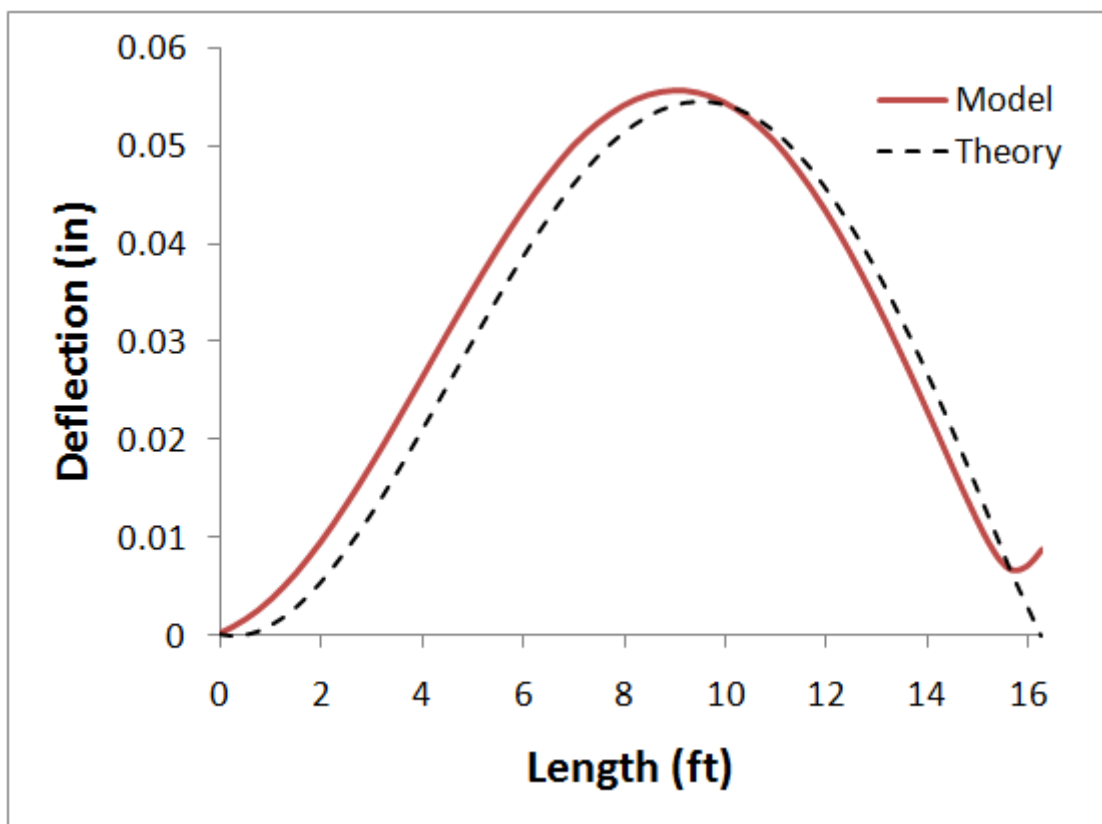
Figure 3.18 – Theoretical deflection vs. finite element analysis deflection.

The maximum deflection computed in the numerical analysis was 0.0556 inches at 8'-11 7/16" from the roadway-approach slab joint while the maximum deflection calculated from the theoretical beam was 0.0545 inches as 9'-5 3/8" form the roadway-approach slab joint.

Differences that exist between the two models can be attributed to the differing boundary conditions placed on the approach slab in the ABAQUS model. The slope of the deflection computed at the beginning of the approach slab is not zero in the numerical analysis. This behavior is the result of the left support of the approach slab not being a truly fixed support. The amount of rotation of this joint in the numerical analysis was $8.13*10^{-5}$ radians. This is significantly larger than the amount of rotation assumed in the theoretical analysis (no rotation is assumed in the theoretical analysis).

The second cause of the difference between the two models is due to the presence of the paving notch. In the numerical analysis, the approach slab initially rested on the paving notch. Deflections occurred as the approach slab was loaded. These deflections caused some rotation of the approach slab at the paving notch support. When these rotations occurred, a portion of the approach slab was lifted off the paving notch. This can be seen in Figure 3.18 by the portion of the model curve that bends upward near the right edge of the graph. The resulting cantilever would create some negative moment in the approach slab which would reduce deflection.

The analyses did, however, prove that the moving tandem used in a step-by-step analysis in the ABAQUS program worked in simulating the effect of a vehicle as it passes over the approach slab. The ABAQUS model was then used in subsequent studies.

Validation - Soil Behavior Modeling

Introduction: The behavior of the soil in the model was compared to a plane strain theoretical solution to check that the modeling technique was appropriate. Boussinesq's method for determining the change in vertical stress for any point (x,z) under a strip foundation was used as the theoretical solution. According to Helwany, loading may be considered as a strip foundation when $L/B > 10$ (Helwany, 2007), with L being the length of the tire and B being the width of the tire. The L/B ratio was approximately 64 for this analysis which satisfied the requirements governing the use of Boussinesq's method for strip foundations. Figure 3.19 identifies all variables used by Boussinesq's method.
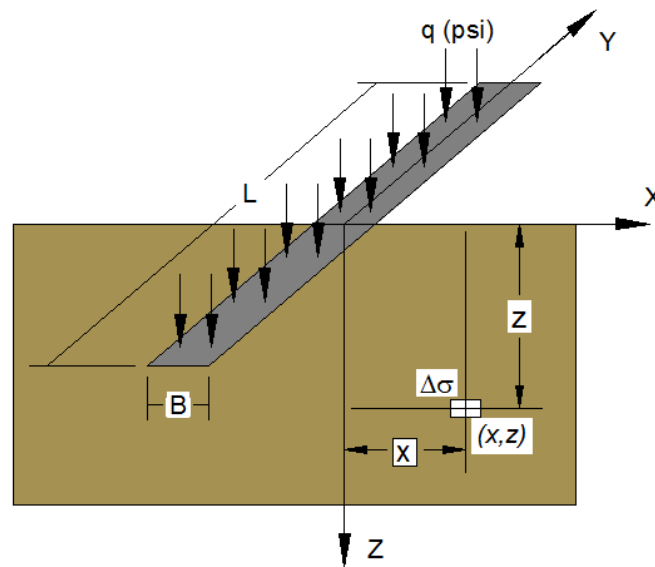
Figure 3.19 – Variables used to analyze strip foundation loads.

Boussinesq's equation, as found in the *Applied Soil Mechanics with ABAQUS Applications* textbook, is presented as Equation 3.2.

$$
\Delta\sigma_z
$$

$$
= \frac{q}{\pi} \left\{ tan^{-1}\left(\frac{x}{z}\right) - tan^{-1}\left(\frac{x-B}{z}\right) + sin\left[tan^{-1}\left(\frac{x}{z}\right) - tan^{-1}\left(\frac{x-B}{z}\right) \right] \right.
$$

$$
\left. * cos\left[tan^{-1}\left(\frac{x}{z}\right) + tan^{-1}\left(\frac{x-B}{z}\right) \right] \right\}
$$

(3.2)

where: $\Delta\sigma_z$ =   Vertical stress increase of point, psi (Pa)

              q   =   Applied pressure

              B   =   Strip load width

              x   =   Horizontal distance of the point from the center of the strip load

              z   =   Vertical distance of the point from the center of the strip load

Loading and Boundary Conditions: Displacement based boundary conditions were placed on the soil and abutment for the validation. Both sides of the soil were restrained

from horizontal displacement while the bottom surface of the soil was restrained from vertical displacement. Boundary conditions placed on the bottom of the abutment prevented rotational, vertical, and horizontal displacements. The boundary condition placed on the base of the abutment simulated a rigid pile and pile connection. Figure 3.20 displays the boundary conditions placed on the soil and abutment.
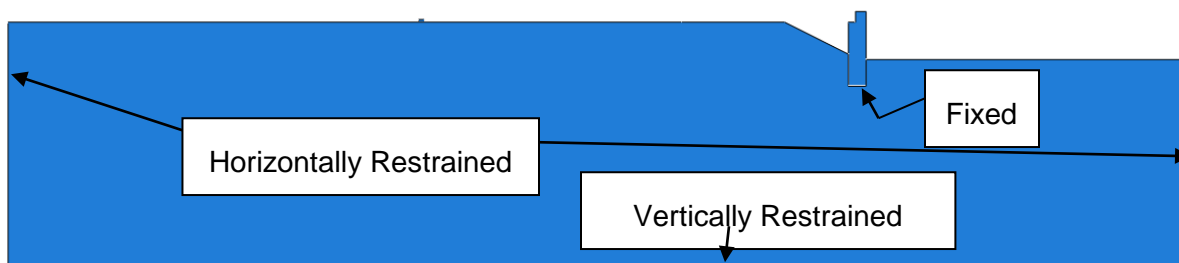
Figure 3.20 – Boundary conditions placed on soil and abutment.

Boundary conditions placed on the tire restricted horizontal displacement for the duration of the analysis. This boundary condition was applied to the left side of the tire as shown in Figure 3.21.
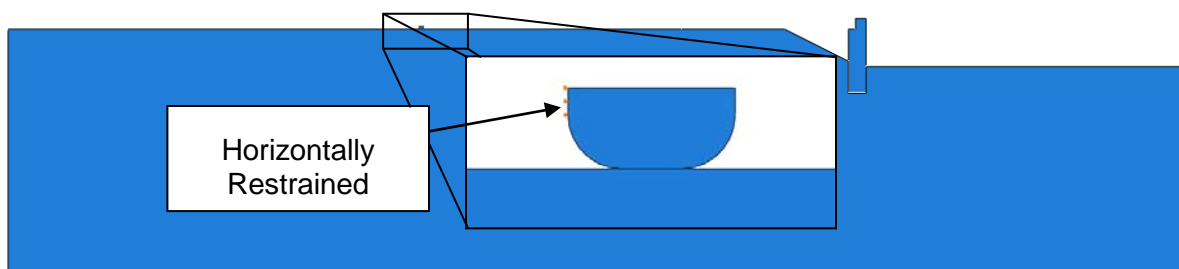
Figure 3.21 – Boundary conditions placed on the tire.

Loading for the verification test consisted of tire loading alone. The width of the tire was taken equal to one lane width (12 ft) as defined by AASHTO. The tire was loaded with a 225 lb. downward force to compress the soil. Figure 3.22 displays the contact surface and loading of the tire.
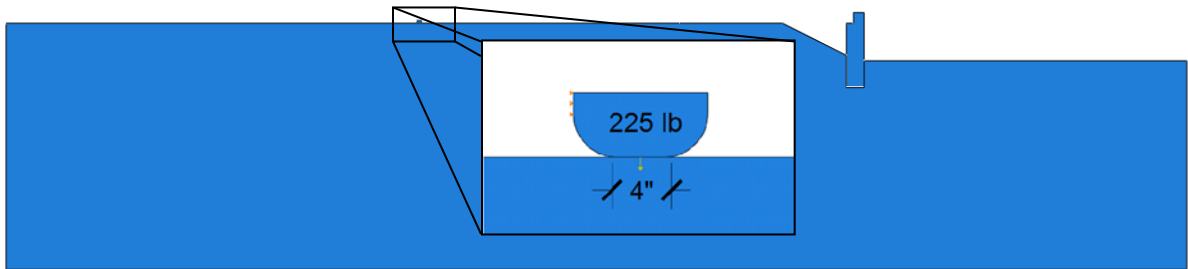
Figure 3.22 – Tire loading use for soil validation.

Results and Discussion: Vertical stress in the soil under the tire as computed from the finite element analysis was compared to vertical stress calculated with Boussinesq's equation for strip foundations. The path feature found within the Abaqus software was used to determine the locations of the elements used for the stress comparison. Figure 3.23 displays the path.
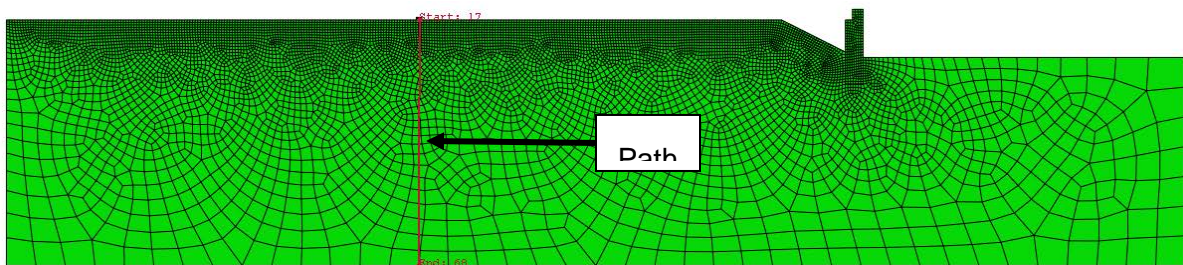
Figure 3.23 – Path used to define elements used for soil validation.

Vertical stress and integration point locations of the elements located along the path were compared to the theoretical vertical stress computed with Boussinesq's equation. Figure 3.24 displays the stress calculated in both the finite element analysis and theoretical equation.
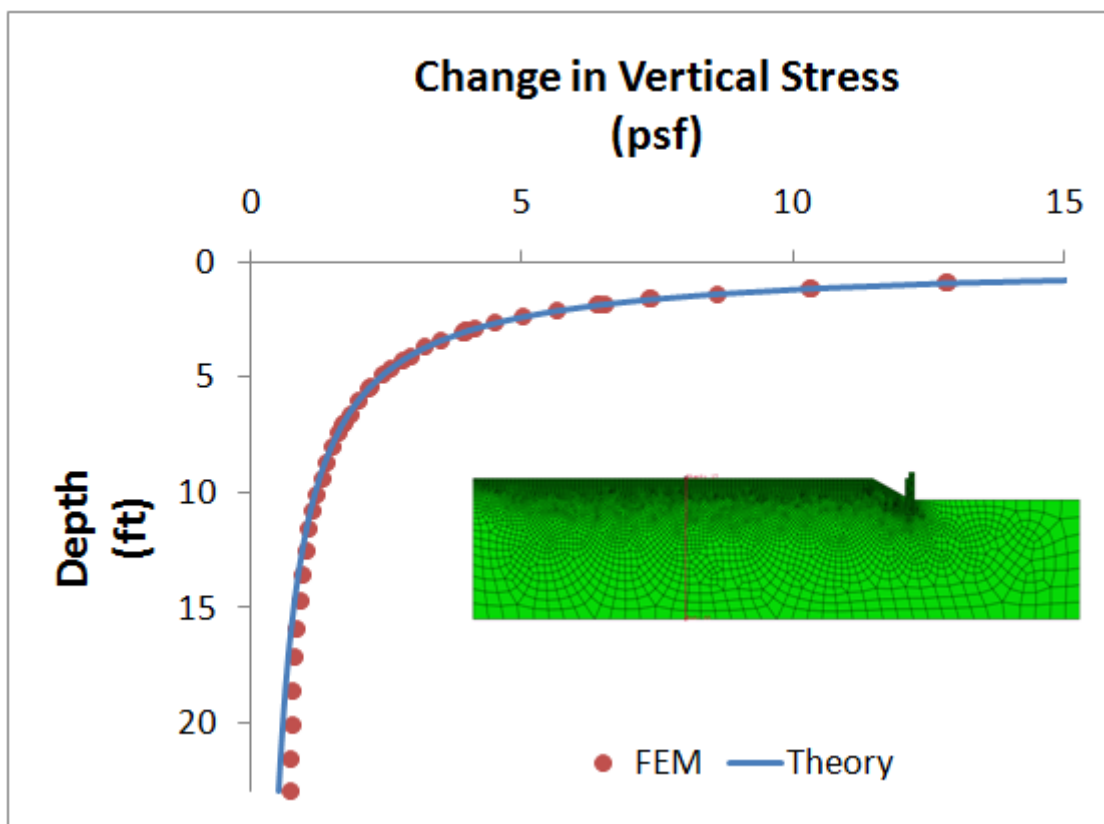
Figure 3.24 – Theoretical stress and finite element analysis stress comparison.

The vertical stress determined from the finite element analysis shows a trend that that matches the theoretical calculations. Less than 10% error existed between the two solutions from the surface to a depth of approximately 11'-6". The error between the two methods gradually increases to a maximum error of 45% at an approximate depth of 23' where the stresses are very low.

Differences between the two methods seen at deeper depths may be due to the boundary conditions imposed on the finite element model. The bottom of the soil was prescribed a boundary condition that restrained vertical displacement. This boundary condition may have caused an abnormal increase in vertical stress near the boundary condition. The theoretical solution only considered the increase in vertical stress from the point load alone and did not have any conditional restraints. The low error (less than 10%) between the two methods observed from the ground surface to a depth of 11'-6" validates the

soil properties and suggests the depth of soil would be adequate to minimize poisoning of the soil from the lower boundary condition.

Model Details

  Soil Properties: The soil was modeled as a compacted sandy soil using the elastoplastic Mohr-Coulomb material model within Abaqus. Compacted sands are common in Wisconsin (Edil, et al., 2007). The sand emulated in the model was Portage Sand as discussed by Schuettpelz et al. (2010). Seven properties were required by Abaqus to define a soil. The seven properties, with appropriate units, were:

- Mass density, lb/in^3 (kg/m3),
- Young's modulus, psi (Pa),
- Poissons ratio,
- Friction angle, degrees,
- Dilation angle, degrees,
- Meridional eccentricity, and
- Cohesion, psi (Pa).

  Soil properties for three cases are summarized in Table 3.2.

<div align="center">

Table 3.2 – Soil properties

</div>

Classification	Mass Density (lbm/ft^3)	Young's Modulus (psi)	Poisson's Ratio	Friction Angle (deg)	Dilation Angle (deg)	Meridional Eccentricity	Cohesion (psi)
Stiff	129	14500	0.3	45	12	0.1	0.145
Moderately Stiff	124	8700	0.3	37	5.6	0.1	0.145
Loose	121	1450	0.3	30	0	0.1	0.145

  Schuettpelz et al. (2010) indicated that Portage sand at a relative compaction of 93% had an equivalent relative density (D_r) of 52%, or it could be considered as a medium dense sand ($0.35 < Dr < 0.65$). At low stresses, the dilation angle (φ) of medium dense sands is often on the order of 5° to 6° (i.e., Bolton 1986), leading to a peak friction angle of 37° for a constant volume (φ'_{cv}) friction angle of 30° ($\theta'_{pk} \approx \theta'_{cv} + 0.8\psi$).

The most critical parameter for the analysis was the Young's modulus (E) of the soil. Young's modulus is often referred to as the elastic modulus. In pavement design, the resilient modulus (M_r) is often used to characterize 'elastic' behavior during cyclic loading. The resilient modulus is conceptually similar to the elastic modulus, except it is based on 'recoverable' strain (ε_r) instead of axial strain. Schuettpelz et al. (2010) illustrated that when corrections are taken into consideration for void ratio, strain level, and stress level, unload-reload resilient modulus are typically higher than (secant) elastic modulus values at low (< 29 ksi) values of E. The 'correction' of Schuettpelz et al. (2010) was used to increase estimated E values to those appropriate for modeling highway base course properties. Figure 3.25 illustrates the difference between the elastic and resilient moduli (Naik, et al., 2006).
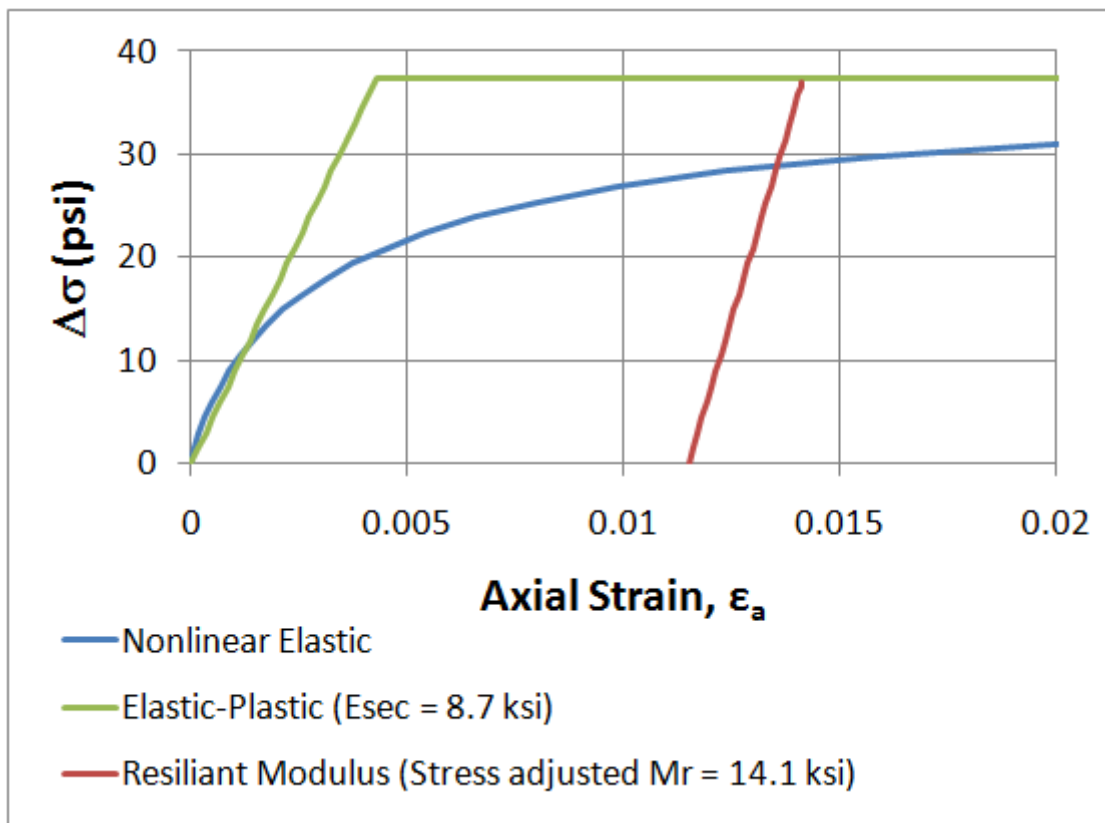
Figure 3.25 – Comparison of nonlinear elastic model with use of secant elastic and secant (stress corrected) resilient moduli.

Concrete Properties: Concrete was modeled using the elastic material model within Abaqus. Four concrete properties needed to be defined in Abaqus for each analysis. The four properties, with appropriate units, were:

- Mass density, lb/in^3 (kg/m^3),
- Concrete compressive strength, psi (Pa),
- Young's' Modulus, psi (Pa), and
- Poissons Ratio.

Table 3.3 displays the concrete properties used to define type 1 and type 2 concrete in the model.

Table 3.3 – Concrete properties

Concrete Type	Density (lb/ft^3)	fc' (psi)	Young's Modulus (ksi)	Poissons Ratio
1	145	4000	3605	0.3
2	145	8000	5098	0.3

The mass density of concrete was determined from recommendations specified in ACI 318-08. According to section 2.2 of ACI 318-08, the density of concrete is typically between 135 pcf and 160 pcf. The density of the concrete was taken from the recommendations provided in ACI 318-08, section C2.2, as 145 pcf $(2300 kg/m^3)$.

The 28 day concrete compressive strength (f_c') for type 1 concrete was based on a report submitted to the Wisconsin Highway Research Program (WHRP). Concrete studied in WHRP 06-14 had an approximate median 28 day compressive strength of 4000 psi (Naik, et al., 2006). Using this information, the 28 day concrete compressive strength used for the analyses was 4000 psi. Type 2 concrete was used to compare the effects of concrete stiffness on the model. A 28 day compressive strength of 8000 psi was used for type 2 concrete.

Young's modulus was determined according to the guidelines presented in section 8.5.1 of ACI 318-08. Section 8.5.1 of ACI 318-08 directs the utilization of Equation 3.3 to determine the modulus of elasticity.

$$E = 57000\sqrt{f_c'} \tag{3.3}$$

where:

E	=	Concrete modulus of elasticity, psi (Pa)
f_c'	=	Concrete compressive stress, psi (Pa)

  The impact of differing Poisson's ratios was explored. An acceptable range of Poisson's ratio for concrete is from 0.15 to 0.25 (Hall, et al., 2008). Analyses were performed with a Poisson's ratio of 0.2 and 0.3 to determine how sensitive the results were to Poisson's ratio. The strain in the approach slab, as determined from each analysis, was then compared. Less than a 1% difference in strain was noticed between the two models. From the Poisson ratio sensitivity study, either value of Poisson's ratio could be used. A Poisson's ratio of 0.3 was adopted for all analyses.

  Reinforcement in the slab, if any, was ignored and the gross moment of inertia was used for all sections unless the concrete cracking strain was exceeded. Concrete cracking stress was determined using the modulus of rupture as defined in section 9.5.2.3 in ACI 318-08. Equation 3.4 displays the equation presented in ACI 318-08 to determine the modulus of rupture.

$$f_r = 7.5\sqrt{f_c'} \tag{3.4}$$

where:

f_r	=	Modulus of rupture (psi)
f_c'	=	Concrete compressive stress (psi)

  Concrete cracking strain was then calculated using Hookes Law. Equation 3.5 displays the Hookes Law relationship used to determine the cracking strain.

$$\varepsilon_{crack} = \frac{f_r}{E} \tag{3.5}$$

where:

$$\varepsilon_{crack} \quad = \qquad \text{Concrete cracking strain (in/in)}$$

$$f_r \qquad = \qquad \text{Modulus of rupture (psi)}$$

$$E \qquad = \qquad \text{Modulus of elasticity (psi)}$$

Strain in the concrete members was compared to the cracking strain after each analysis. The moment of inertia was modified for all concrete members that exceeded the cracking strain and the analysis was repeated. The moment of inertia of the cracked section was modified to be 66% of the gross moment of inertia. The resulting strain from the repeated analysis was again compared to the cracking strain as determined by Equation 3.5.

Abutment: The abutment used in the Abaqus model was designed to geometrically conform to the A5 abutment described in the WisDOT standard specifications. The abutment incorporated a standard WisDOT paving notch to support the approach slab. Figure 3.26 displays the geometry used to define the abutment in Abaqus.
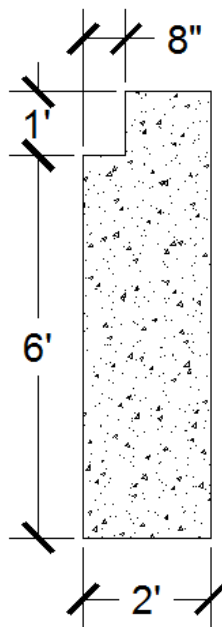

Figure 3.26 – Abutment geometry.

All analyses utilized the concrete previously identified at Type 1 concrete ($f_c' = 4000$ psi) for the abutment and neglected all superstructure loads placed on the abutment.

Roadway: The cross-sectional area of the roadway was determined using guidelines outlined in AASHTO. The width of the roadway was equal to the minimum recommended lane width (12'. Thickness was maintained at a constant 1' throughout the length of the roadway.

In order to ensure that the soil away from the approach slab can deform normally during the truck loading, several analysis iterations of models with varying roadway length were conducted. From these analyses, it was determined that the roadway in front of the approach slab needed to be a minimum of 58' long to avoid any disturbance of the soil beneath the approach slab during the initial design truck loading. The minimum length of the roadway analyzed in Abaqus was 59' for all of the analysis cases investigated.

All analyses utilized the roadway concrete previously identified in the concrete properties section as Type 1 concrete (f_c' = 4000 psi).

Approach Slab: The non-skewed approach slab analyzed in the model was made to conform to WisDOT standard specifications. WisDOT uses a length of 15'-8" and a thickness of 1ft for the standard approach slab. The initial analysis utilized the concrete previously identified in the concrete properties section as Type 1 concrete (fc' = 4000 psi).

Interaction: Friction was the primary constraint utilized in the model to control all concrete-to-concrete and soil-to-concrete interactions. The coefficient of friction used to define all concrete-to-concrete interactions was taken from section 11.6.4.3 of ACI 318-08. It was assumed that each concrete member was placed against hardened concrete that was not intentionally roughened. Using this assumption, the coefficient of friction (μconc) was equal to 0.6. The coefficient of friction used to define the soil to concrete interaction was 0.577 (Jardine, et al., 1993).

A coupling restraint was placed at the roadway-approach slab interface. The coupling allowed rotation between the two parts but prevented both horizontal and vertical displacement of the approach slab relative to the roadway. This coupling was placed at the quarter point down from the top of the approach slab. Figure 3.27 displays the location of the coupling between the roadway and approach slab.
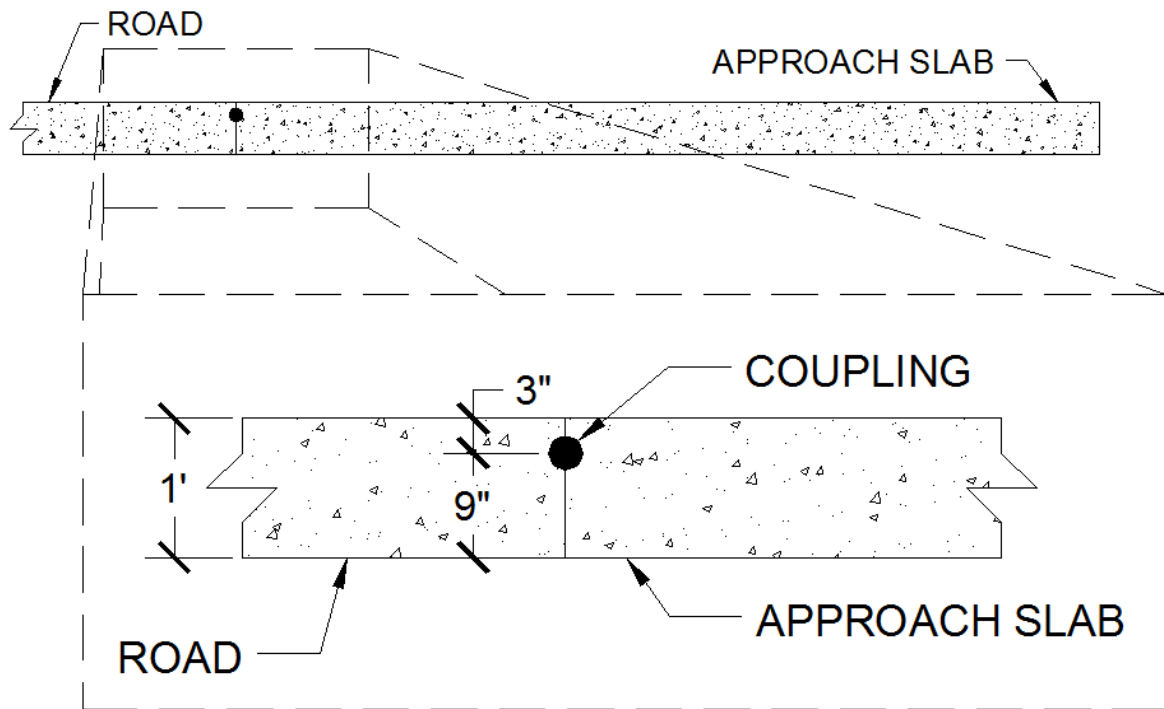
Figure 3.27 – Roadway-approach slab coupling location.

Boundary Conditions: Boundary conditions imposed on the fill were determined using recommendations provided by Seos (Seo, 2003). Seo recommends a 22'-11 ½" (7 m) minimum depth of soil to minimize the adverse effects of boundary condition poisoning. The depth of the soil complied with the recommendations provided by Seo. A vertical displacement restraint was implemented at the bottom of the fill to simulate a stiff natural soil under the fill. Horizontal displacement restraints were placed at the sides of the fill. These boundary conditions did have an effect on the displacement of the roadway near the edge of the model but the impact of this on the approach slab was minimal due to the 59 ft. length of the roadway. Figure 3.28 displays the boundary conditions placed on the model.
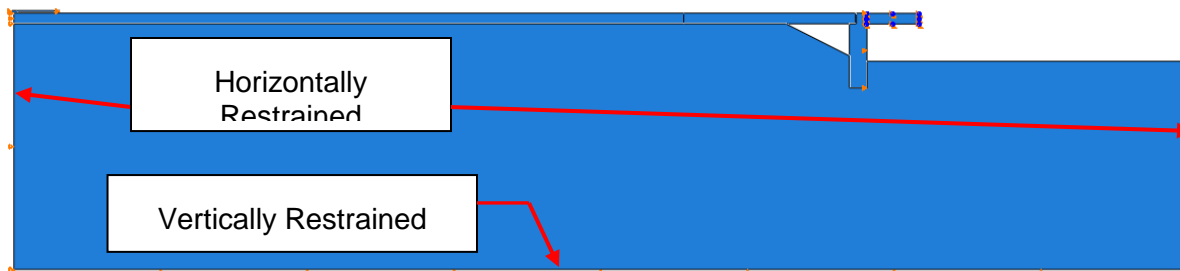
Figure 3.28 – Boundary conditions placed on the soil.

A horizontal displacement boundary condition was placed on the end of the roadway. This boundary condition simulated the remaining portion of the roadway not modeled. Figure 3.29 displays the location of this boundary condition.
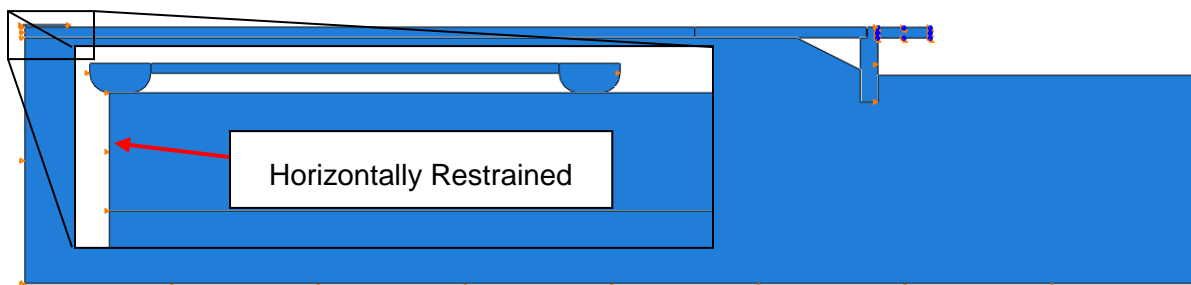
Figure 3.29 – Roadway boundary condition location.

Boundary conditions on the abutment were varied depending on the analysis step. Initial boundary conditions were placed on the side of the abutment that allowed vertical displacement while gravity was applied to the model to create soil subsidence. Figure 3.30 displays this initial boundary condition placed on the abutment.
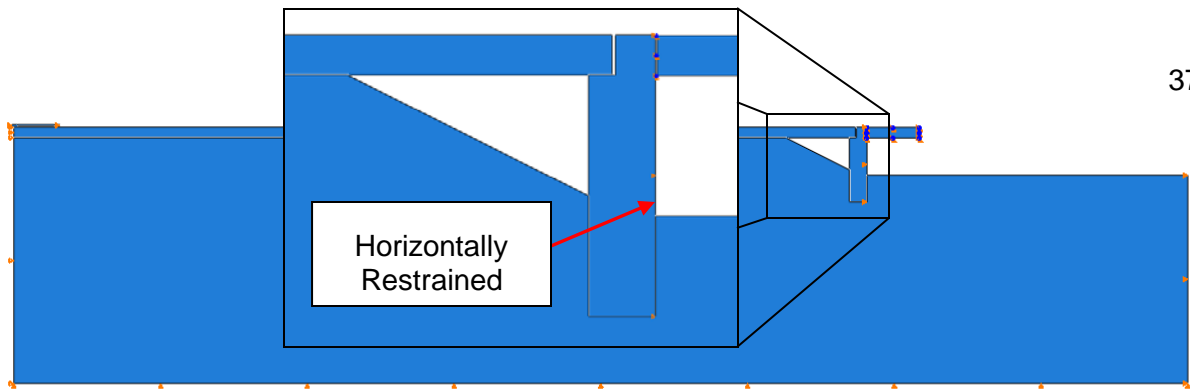
Figure 3.30 – Initial boundary conditions placed on the abutment.

The boundary condition placed on the side of the abutment was removed after gravity had been applied to the model. The next step in the analysis fixed the bottom of the abutment to simulate a rigid pile and pile connection. The flexibility of the pile or connection between the pile and abutment was not considered in any analysis.

The boundary conditions placed on the truck varied depending on the analysis step. Premature movement of the truck during gravity loading was controlled by a horizontal restraint placed on the tires of the truck. This boundary condition remained in effect until the HL93 tandem truck axle loads were applied to the 'tires'. Figure 3.31 displays the location of the initial boundary conditions prescribed on the 'tires' of the truck.

Figure 3.31 – Modeled truck initial boundary conditions.

A second boundary condition applied to the entire truck invoked a controlled horizontal displacement. The truck moved horizontally across the roadway and approach slab in 4" maximum increments. Abaqus was allowed to automatically reduce this increment if convergence problems were encountered during the analysis. Figure 3.32 displays the final location of the truck after it moved from the roadway (at left) and across the approach, then on to the bridge.
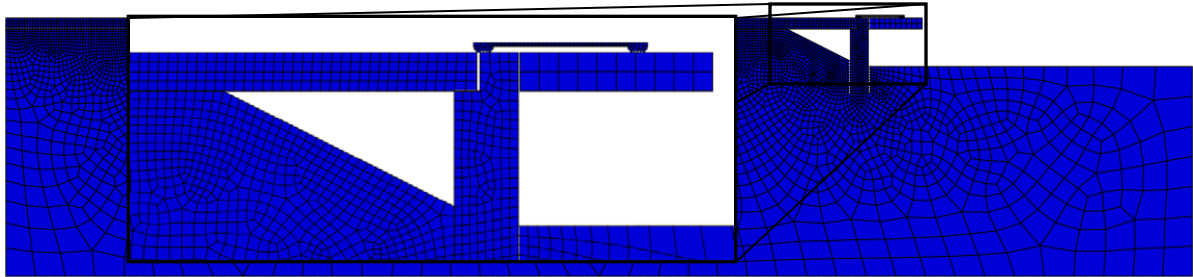
Figure 3.32 – Final location of truck – on the bridge.

Initial boundary conditions were prescribed on the bridge restricted horizontal, vertical, and rotational displacement. Boundary conditions initially placed on the bridge remained in effect throughout the analysis.

Loading: The first analysis step applied gravity to the model to allow soil subsidence. This loading was used for each analysis.

Axle loads applied by the modeled truck conformed to the HL93 tandem design truck outlined by AASHTO. AASHTO specified two 25 kip axle loads spaced 4' apart for the HL93 tandem design truck. These axle loads were kept constant while the truck was moved along the roadway and approach slab. Figure 3.33 displays the axle loading and spacing modeled after the design truck.
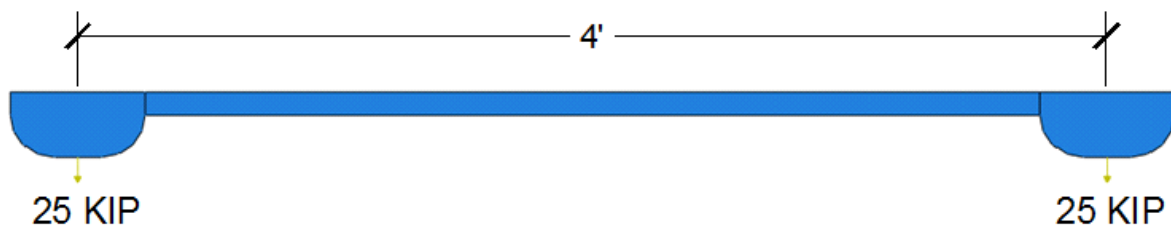
Figure 3.33 – Modeled truck with HL93 axle loading.

A separate analysis was performed that considered gravity and lane loading alone. This analysis utilized a vertical distributed load with a magnitude of 640 lb/ft as defined by AASHTO. The lane load was applied to entire length of the roadway and approach slab.

Mesh: The model utilized multiple meshing schemes. Nodal seeding of all concrete parts was governed by size. This seeding ensured the creation of uniformly sized elements. Seeding of the soil fill was governed by a combination of size and biased seeding techniques. The size of the seeds that were in contact with concrete and the bottom of the fill were governed by size. Biased seeding techniques were used on the edges of the fill and on the fill under the bridge. Figure 3.34 identifies the locations on the fill where the differing seeding techniques were used. Figure 3.35 displays the mesh used to analyze the model.
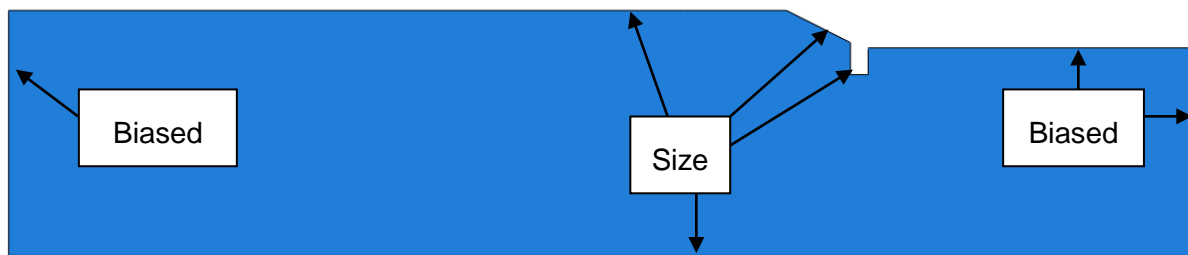
Figure 3.34 – Seeding techniques used to define the mesh on the fill.
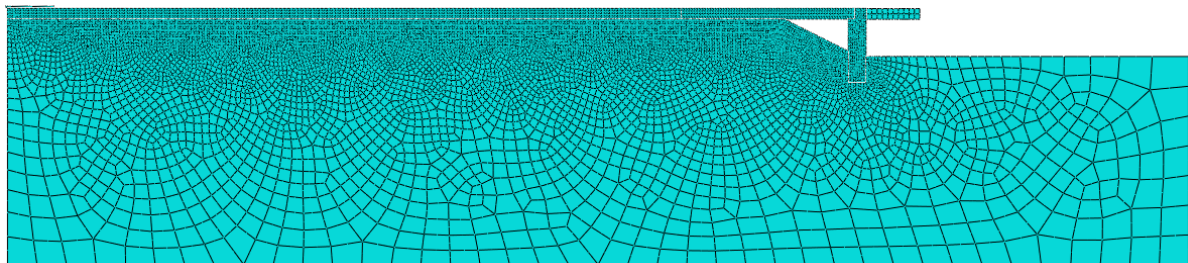
Figure 3.35 – Mesh used in the model.

Elements: Plane strain and plane stress elements were used in the model. Plane strain quadrilateral quadratic elements with reduced integration were used for the soil region (Helwany, 2007). Plane stress quadrilateral quadratic elements with reduced integration were used for all concrete parts.

Mesh Refinement Study: A mesh refinement study was performed to determine an acceptable mesh density. The mesh refinement study utilized Richardson's extrapolation formula to determine a quantity of interest calculated with an infinitely fine mesh (Cook, et al., 2002). Richardson's extrapolation formula is shown as Equation 3.6.

$$\phi_\infty = \frac{\phi_1 h_2^q - \phi_2 h_1^q}{h_2^q - h_1^q} \tag{3.6}$$

where: ϕ_∞ = Quantity from infinite mesh

ϕ_1 = Quantity from 1st mesh

h_2 = Characteristic length *(longest line segment that fits within an element)* of 2nd mesh

q = Extrapolation exponent

ϕ_2 = Quantity from 2nd mesh

h_1 = Characteristic length of 1st mesh

Multiple analyses conducted with a minimum of three different sized mesh densities were required to use Richardson's extrapolation formula. Analyses were conducted with 1.5", 3", and 6" sized elements (the length of one side of the element) on the approach slab. Figures 3.36 – 3.38 display the meshes used in the mesh refinement study.
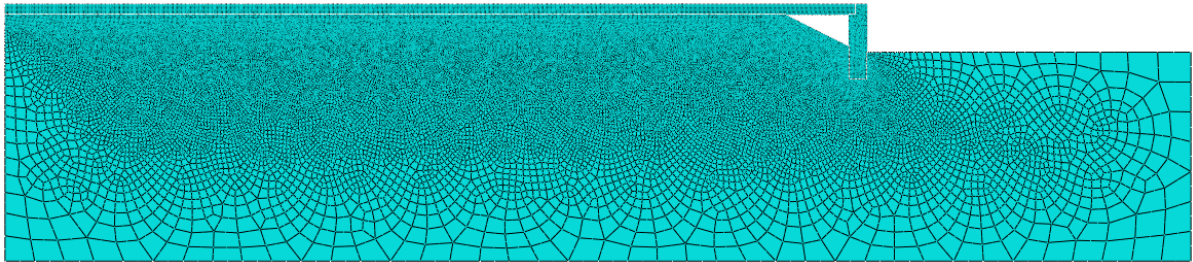
Figure 3.36 – 1.5" elements used in mesh refinement study.
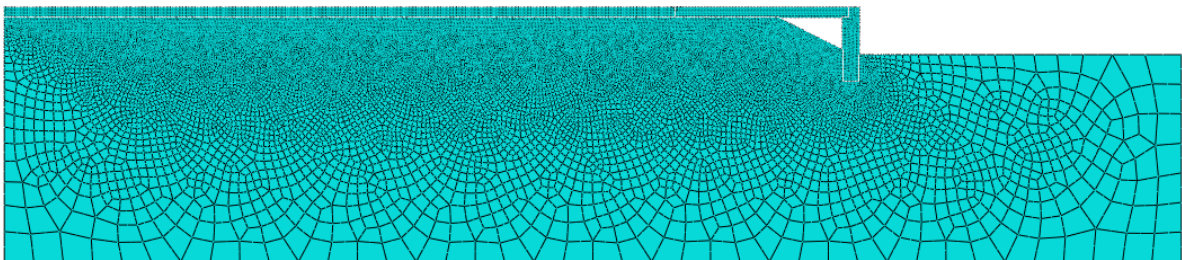
Figure 3.37 – 3" elements used in mesh refinement study.
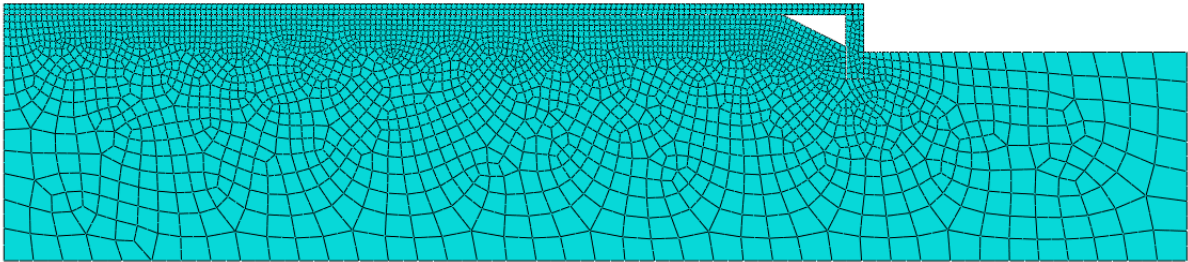
Figure 3.38 – 6" elements used in mesh refinement study.

The deflection of the approach slab was used as the quantity to compare the effect of mesh densit. The bottom corner of the approach slab, near the roadway, was selected as the point that would be used for the comparison. Figure 3.39 displays the location of the point used in all comparisons.
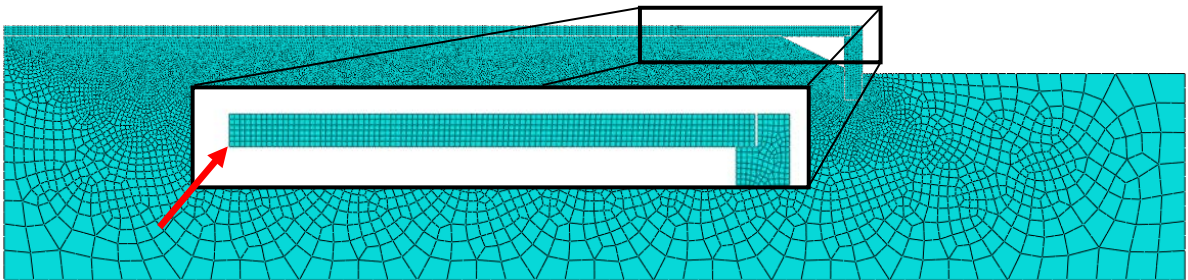
Figure 3.39 – Control point used in mesh refinement study.

The extrapolation exponent (q) was determined using methods outlined by the Cook (Cook, et al., 2002). Cook recommended finding the value of q graphically. Deflection (φ) taken at the control point identified in Figure 3.38 was plotted against the characteristic length (h) raised to the q power. The value of q was altered until the plot of φ vs. h^q plotted a straight line. A value of 2.47 for q was used to plot the straight line.   Figure 3.40 displays the plot used to determine q.
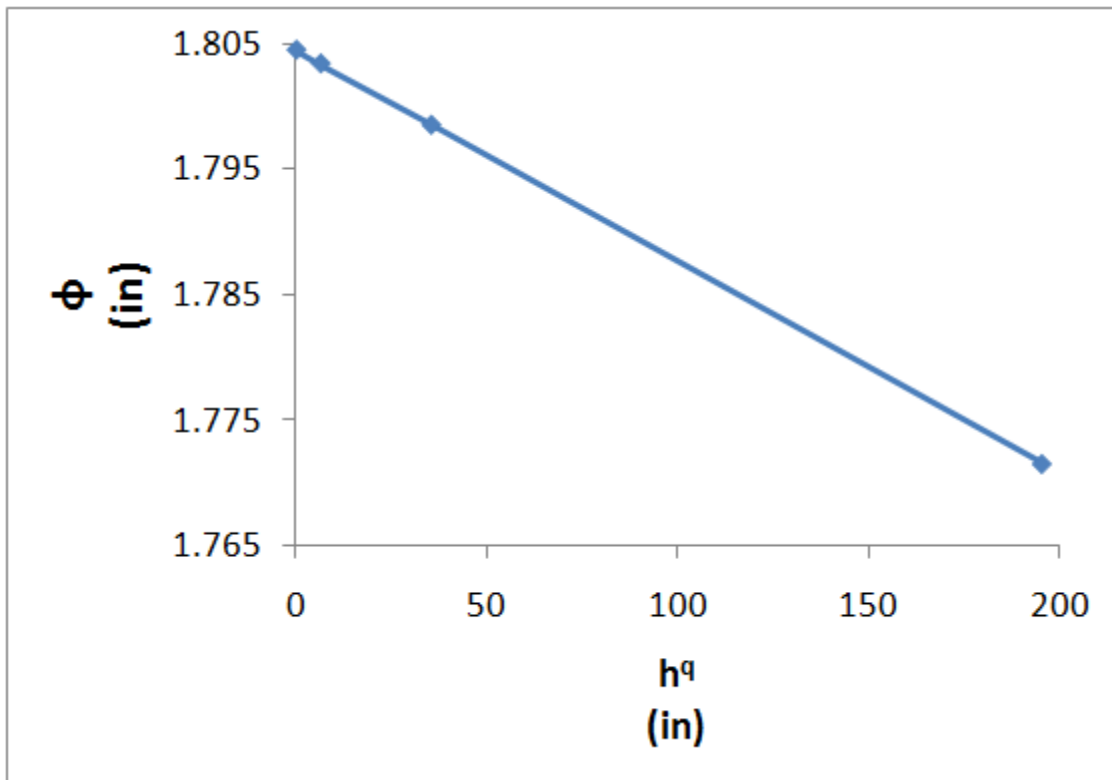
Figure 3.40 – hq vs. φ plot used to determine q for Richardson's extrapolation.

The displacement of the point with an infinitely fine mesh could be extrapolated by Equation 3.6 and the variables found above. Equation 3.6 yielded a displacement of 1.804".

The error between the extrapolated displacement and the model containing the 1.5" elements was calculated to determine the accuracy of the model. Error was determined using the percent error formula. This formula is presented as Equation 3.7. The calculated error between the model with 1.5" elements and the same model with an infinitely small mesh was 0.06%.

$$e_2 = \frac{\phi_2 - \phi_\infty}{\phi_\infty} \times 100\% \tag{3.7}$$

where: e_2 =   Error in 2nd mesh

ϕ_2 =   Deflection from 2nd mesh

ϕ_∞ =   Deflection from infinite mesh

Richardson's extrapolation formula was applied to the model with 3" elements. The runtime of the model with 3" elements was reduced by approximately 1.5 hours when compared to the model with 1.5" elements. The calculation steps previously defined resulted in a 0.33% error between the model with 3" elements and the model with an infinitely fine mesh. This mesh was used for all subsequent analyses.

Parametric Studies: A series of parametric studies was performed to determine which variables had the largest impact on concrete cracking and end rotation of the approach slab near the abutment. The parameters investigated were:

- Settlement Trench / Void Geometry,
- Approach Slab Length,
- Abutment Height,
- Soil Stiffness,
- Concrete Stiffness, and
- Approach Slab-Roadway Joint Restrictions.

Baseline Model and Parameter Variation

All parametric studies were variations of an established baseline model unless otherwise noted. In the parametric studies only one parameter was varied at a time, unless specifically noted. The characteristics of each part of the baseline model were:

- Soil
  - One homogeneous layer of moderately stiff soil
  - Settlement trench geometry
    - 1ft vertical gap
    - 2ft horizontal gap
- Abutment
  - 6ft height (measured from bottom of approach slab to base of abutment)
  - 4 ksi concrete

- Approach slab
    - 15'-8" length
    - 1ft thick
    - 4 ksi concrete
    - Shear coupling placed at quarter point utilized to connect approach slab to roadway
- Roadway
    - 59ft minimum length
    - 1ft thick
    - 4 ksi concrete
- Truck
    - AASHTO HL93 tandem design truck axle spacing and loads
- Bridge
    - Rigid material
    - Fixed boundary conditions.

Settlement Trench / Void Geometry: The geometry of the settlement trench formed under the approach slab was varied in this parametric study. Settlement trench geometries analyzed are shown in Figure 3.41.

X (ft)	Y (ft)
0	0
2	1
4	2
6	3
8	4

Each settlement trench will have angles congruent to this triangle.
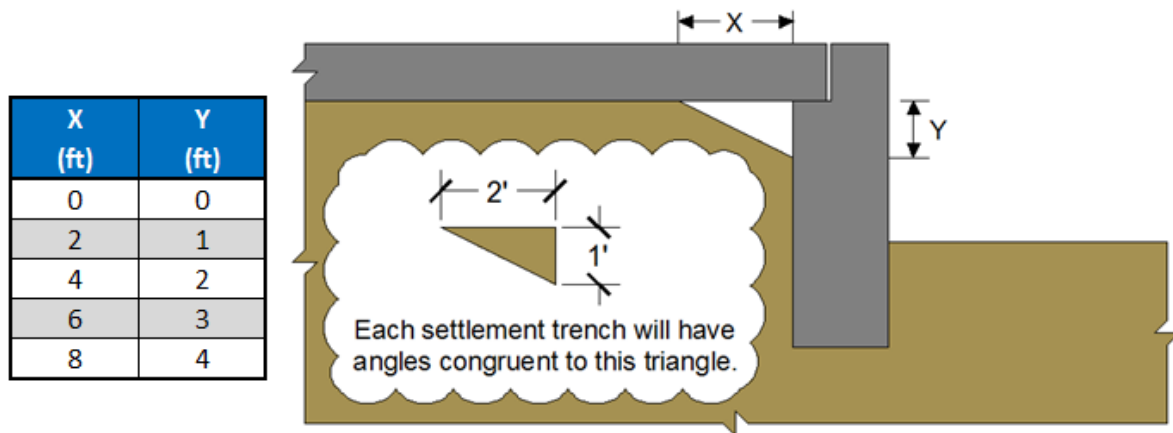
Figure 3.41 – Settlement trench geometries considered in parametric study.

Approach Slab Length: Differing approach slab lengths were analyzed to determine the impact on concrete cracking and end rotation of the approach slab near the abutment. Approach slabs of 10ft and 20ft were analyzed in addition to the baseline model of 15ft-8in. The length of the roadway was modified to accommodate differing approach slab lengths. Roadway length did not violate the recommended length of 58' that was determined previously.

Abutment Height: Two differing abutment heights were analyzed to determine their effect on the approach slab. Abutment heights of 8' and 12' were considered in addition to the 6' high abutment used in the base model.

Soil Stiffness: The stiffness of the soil under the concrete parts was varied to include a layered soil profile and homogeneous layers of loose and stiff soil. Homogeneous soil layer properties are displayed in Table 3.4.

Table 3.4 – Homogeneous soil layer properties.

Classification	Mass Density (lbm/ft^3)	Young's Modulus (psi)	Poisson's Ratio	Friction Angle (deg)	Dilation Angle (deg)	Meridional Eccentricity	Cohesion (psi)
Stiff	129	14500	0.3	45	12	0.1	0.145
Moderately Stiff	124	8700	0.3	37	5.6	0.1	0.145
Loose	121	1450	0.3	30	0	0.1	0.145

The homogeneous soil layers properties do not reflect changes in effective stress with respect to depth and assume uniform compaction throughout the entire layer. A layered soil profile that simulated a stiff soil over loose soil model was analyzed in addition to the homogeneous soil layer analyses to account for changes in effective stress with depth. A graphical representation of the soil layering and a table displaying the layered soil properties is displayed as Figure 3.42 and Table 3.5, respectively.

Figure 3.42 – Layered soil profile.

Table 3.5 – Layered soil properties.

Layer	Depth (ft)	Mass Density (lbm/ft³)	Young's Modulus (psi)	Poisson's Ratio	Friction Angle (deg)	Dilation Angle (deg)	Meridional Eccentricity	Cohesion (psi)
1	1.0	124	8700	0.3	37	5.6	0.1	0.145
2	2.3	122	3625	0.3	32.1	1.68	0.1	0.145
3	6.6	123	5800	0.3	34.2	3.36	0.1	0.145
4	23.0	124	8700	0.3	37	5.6	0.1	0.145

Concrete Stiffness: The stiffness of the approach slab was manipulated with the loose homogeneous soil analysis to test the influence of stiffer concrete. The baseline used the type 1 concrete as defined in Table 3.6. This parametric study utilized concrete type 2, shown in Table 3.6, to define the concrete properties of the approach slab alone. All other concrete members utilized type 1 concrete.

Table 3.6 – Concrete properties used in concrete stiffness parametric study

Concrete Type	Density (lb/ft³)	fc' (psi)	Young's Modulus (ksi)	Poissons Ratio
1	145	4000	3605	0.3
2	145	8000	5098	0.3

Joint Restrictions: Coupling constraints applied to the approach slab at the roadway-approach slab interface were varied from the baseline model to determine how they influenced the behavior of the approach slab. The coupling used on the baseline model allowed rotation but restricted horizontal and vertical displacement of the approach slab

relative to the roadway. An unrestricted and moment coupling was analyzed and compared to the baseline model. The moment coupling restricted rotational, vertical, and horizontal displacement of the approach slab relative to the roadway. Surface-to-surface friction was the only constraint allowed for the unrestricted coupling case. The control point of the coupling is shown in Figure 3.43.
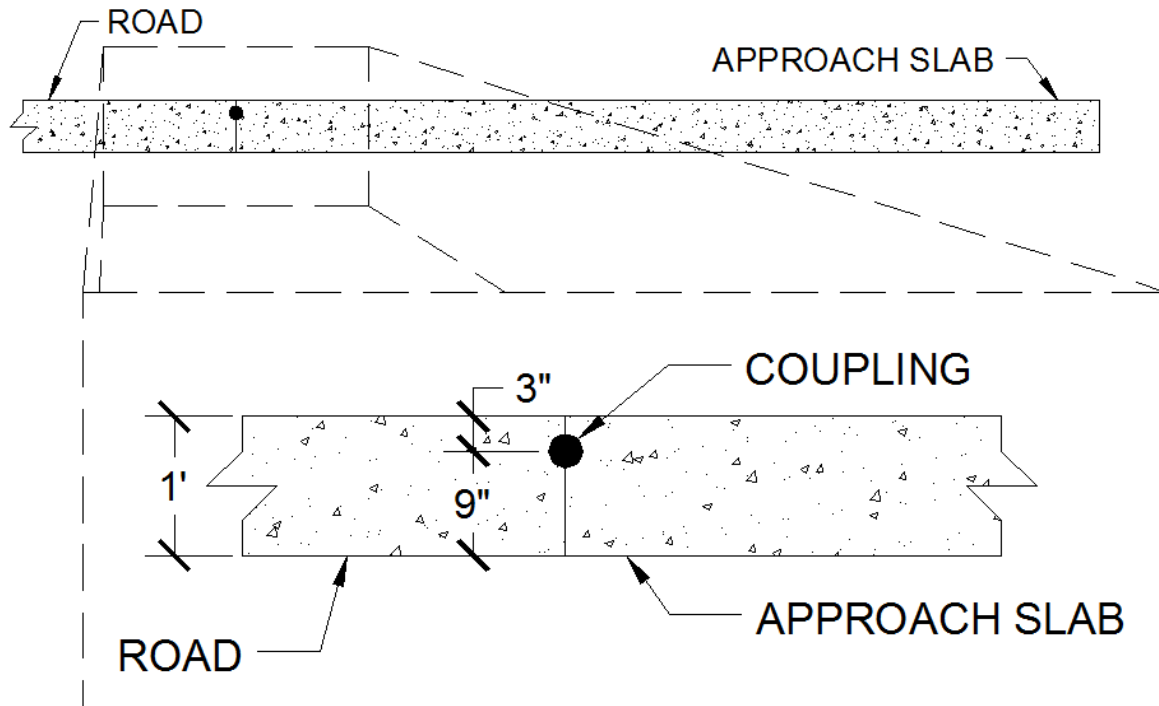
Figure 3.43 – Roadway-approach slab coupling location.

4. Analysis Results

Introduction

Flexural strains developed in the approach slab and end rotation at the abutment joint were used as the bases for classifying the behavior as the design parameters were varied. Envelopes of the maximum (tensile) and minimum (compressive) principle strains were created for nodes located along the top and bottom fiber of the approach slab. The compressive strain was compared to the concrete crushing strain defined in ACI 318-08. Tensile strains were compared with the rupture strain to determine if cracking had occurred.

A datum point was located at the joint between the roadway and approach slab. All resulting strain plots use this point as datum. Figure 4.1 displays datum and the coordinate system used in the interpretation of all results.
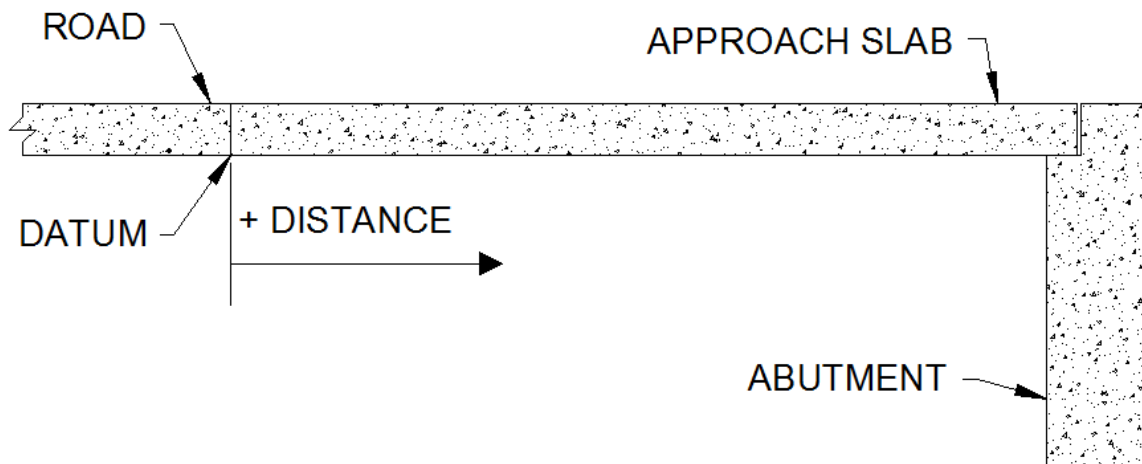
Figure 4.1 – Coordinate system used to interpret results.

The concrete cracking strain was determined using a combination of the guidelines outlined in ACI 318-08 and Hooke's Law. Equation 4.1 displays the equation used to determine the concrete cracking strain.

$$\varepsilon_{crack} = \frac{7.5\sqrt{f_c'}}{E}$$ (4.1)

where:

ε_{crack} =   Concrete cracking strain (in/in)

f_c' =   Concrete compressive stress (psi)

E   =   Concrete modulus of elasticity (psi)

The crushing strain was taken as 0.003 as defined in the ACI 318-08. None of the analysis exhibited concrete crushing.

Displacements of the top and bottom nodes located along the vertical edge of the approach slab were used to determine end rotation. The rotation of the joint near the abutment was determined for each analysis case. Rotation of the approach slab located near the roadway was determined for one analysis case only.

Base Model Behavior

Base Model Results: The base model did not exhibit any cracking of the approach slab and the maximum rotation of the joint near the abutment was 0.001086 radians. The minimum principle (compressive) strain in the approach slab was 0.0000904 in/in at a distance of 11'-9" from datum. The maximum principle (tensile) strain was 0.0000823 in/in at 11'-2 ¼" from datum. Figure 4.2 displays the tensile strain envelope of the bottom surface of the approach slab.
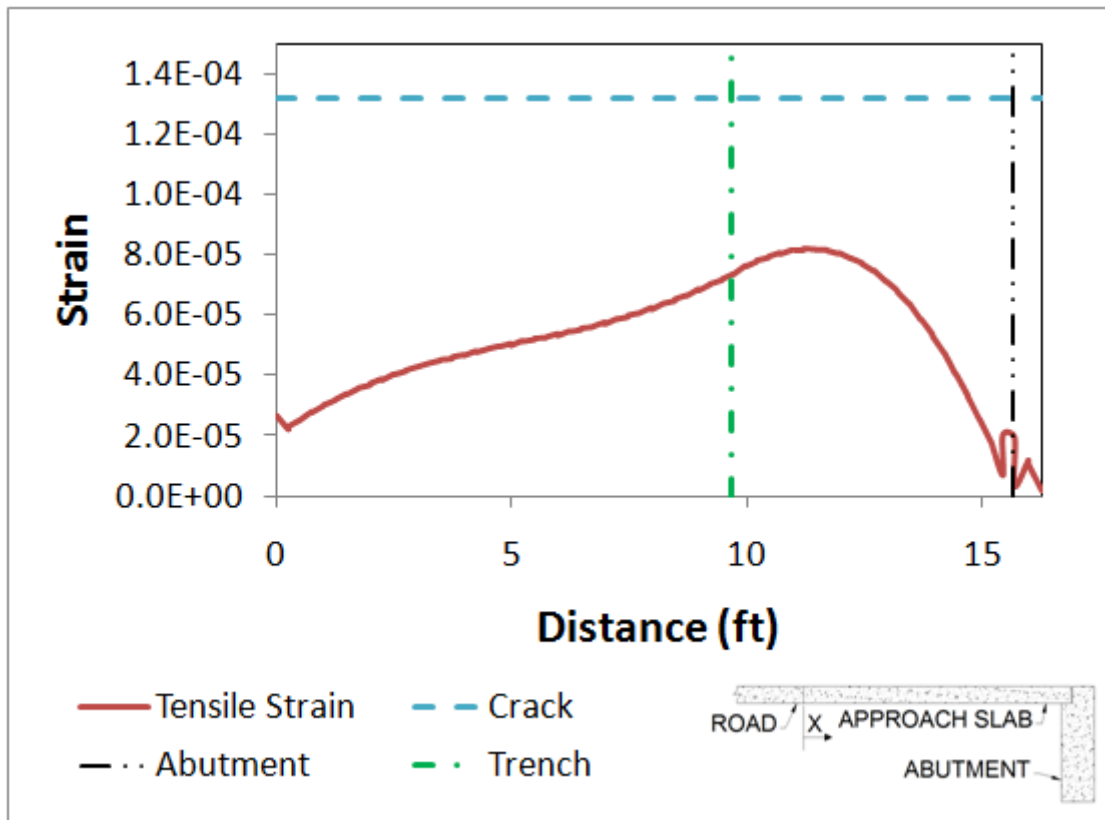
Figure 4.2 – Maximum principle (tensile) strain envelope for the baseline slab.

Results from lane loading: Strains and rotation of the approach slab were determined from the model consisting of lane loading alone. The lane loading analysis incorporated the standard 640 lb/ft distributed load placed along the entire length of the roadway and approach slab as defined in the 2008 AASHTO design code. The largest maximum principle (tensile) strain in the approach slab was 0.0000362 in/in measured at 11'-2 ¼" from datum. The maximum rotation of the joint between the approach slab and abutment was 0.000796 radians. The largest minimum principle (compressive) strain in the approach slab was 0.0000376 in/in at 11'-3" from datum. Figure 4.3 displays the maximum principle strain envelope for the bottom fiber of the approach slab.
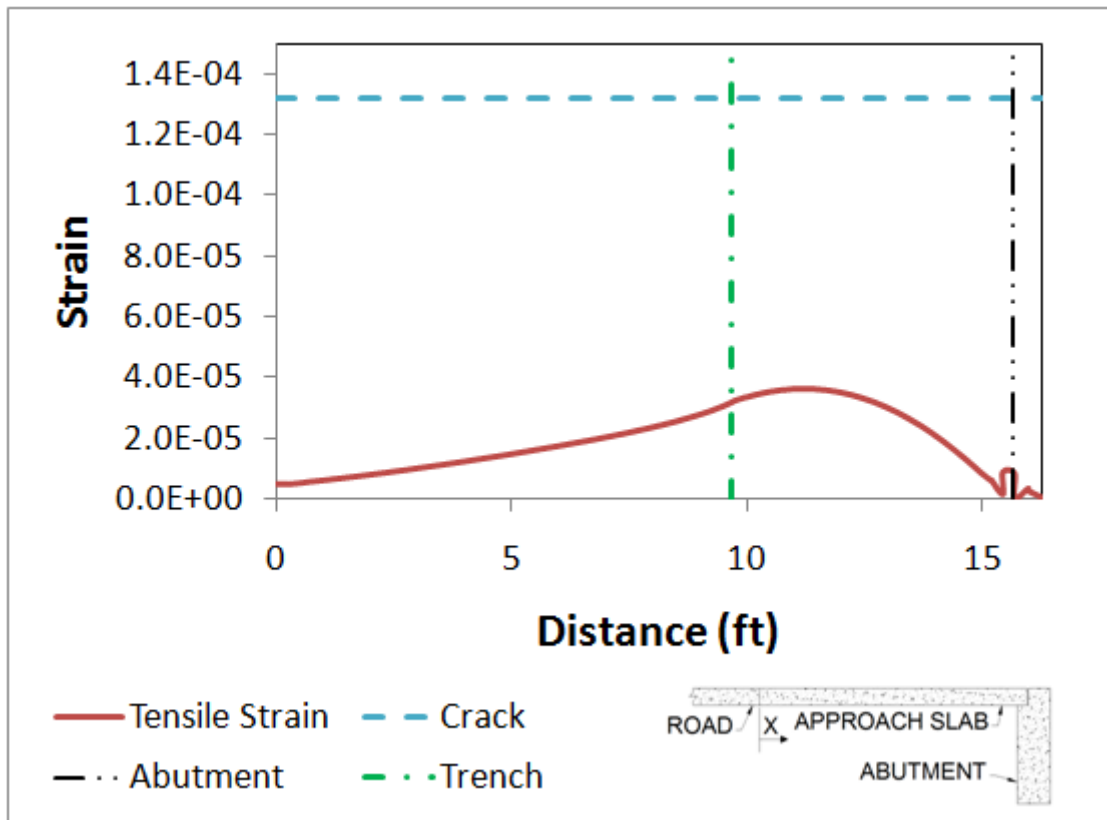
Figure 4.3 – Maximum principle strain of approach slab under lane loading.

Results from parametric studies

Fill Properties: Soil properties were varied to encompass the upper and lower bounds of the soil that may exist under the approach slab. A total of four different analyses were conducted with different soil properties. Three of these analyses assumed a homogeneous soil layer under the roadway and approach slab. The homogeneous soil layer varied the density, modulus of elasticity, friction angle, and dilation angle for each analysis case. Table 4.1 shows the soil properties used for homogeneous soil layered analysis cases.

Table 4.1 – Homogenous soil layered analysis properties.

Classification	Mass Density (lbm/ft³)	Young's Modulus (psi)	Poisson's Ratio	Friction Angle (deg)	Dilation Angle (deg)	Meridional Eccentricity	Cohesion (psi)
Stiff	129	14500	0.3	45	12	0.1	0.145
Med.	124	8700	0.3	37	5.6	0.1	0.145
Loose	121	1450	0.3	30	0	0.1	0.145

An additional analysis was performed with a layered soil profile that accounted for changes in effective stress with depth. The layered soil profile mimicked a stiff-over-soft-over-stiff layering scheme. Layer 1 was the surface layer of the model while Layer 4 was the deepest soil layer in the model. Table 4.2 displays the thickness and soil properties for each layer. Figure 4.4 displays the layered soil model and identifies the soil layer numbering scheme.

Table 4.2 – Layered soil analysis properties.

Layer *	Depth (ft)	Mass Density (lbm/ft³)	Young's Modulus (psi)	Poisson's Ratio	Friction Angle (deg)	Dilation Angle (deg)	Meridional Eccentricity	Cohesion (psi)
1	1.0	124	8700	0.3	37	5.6	0.1	0.145
2	2.3	122	3625	0.3	32.1	1.68	0.1	0.145
3	6.6	123	5800	0.3	34.2	3.36	0.1	0.145
4	23.0	124	8700	0.3	37	5.6	0.1	0.145

Layer 1 is the upper-most layer. The numbering increases with increasing depth.
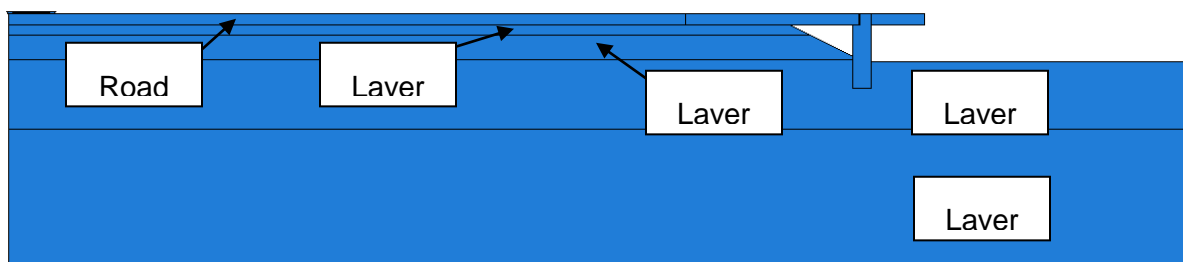
Figure 4.4 – Layered soil analysis.

The loose homogeneous soil layer case was the only case where cracking occurred. For this case, the moment of inertia of the cracked section was modified according to ACI 318-08 to represent a cracked moment of inertia. The analysis was performed again and was repeated until only the region of the approach slab that had exceeded the cracking strain had the cracked moment of inertia. Figure 4.5 displays the final maximum principle strains along the bottom of the approach slab. Table 4.3 displays the location and magnitude of the maximum (tensile) principle strains calculated from this parametric study. Table 4.4 displays the location and magnitude of the minimum (compressive) principle strains calculated from this parametric study.

Table 4.3 – Maximum principle (tensile) strains with location for soil parametric study.

Case	Strain	Location
Stiff Soil	7.06E-05	11'-8 1/4"
Moderately Stiff	8.23E-05	11'-2 1/4"
Layered Soil	9.36E-05	10'-11 1/4"
Loose Soil	3.29E-04	10'-2 3/8"

Table 4.4 – Minimum principle (compressive) strains with location for soil parametric study.

Case	Strain	Location
Stiff Soil	-7.97E-05	11'-9"
Moderately Stiff	-9.04E-05	11'-9"
Layered Soil	-1.02E-04	11'-3"
Loose Soil	-3.63E-04	10'-11 1/4"
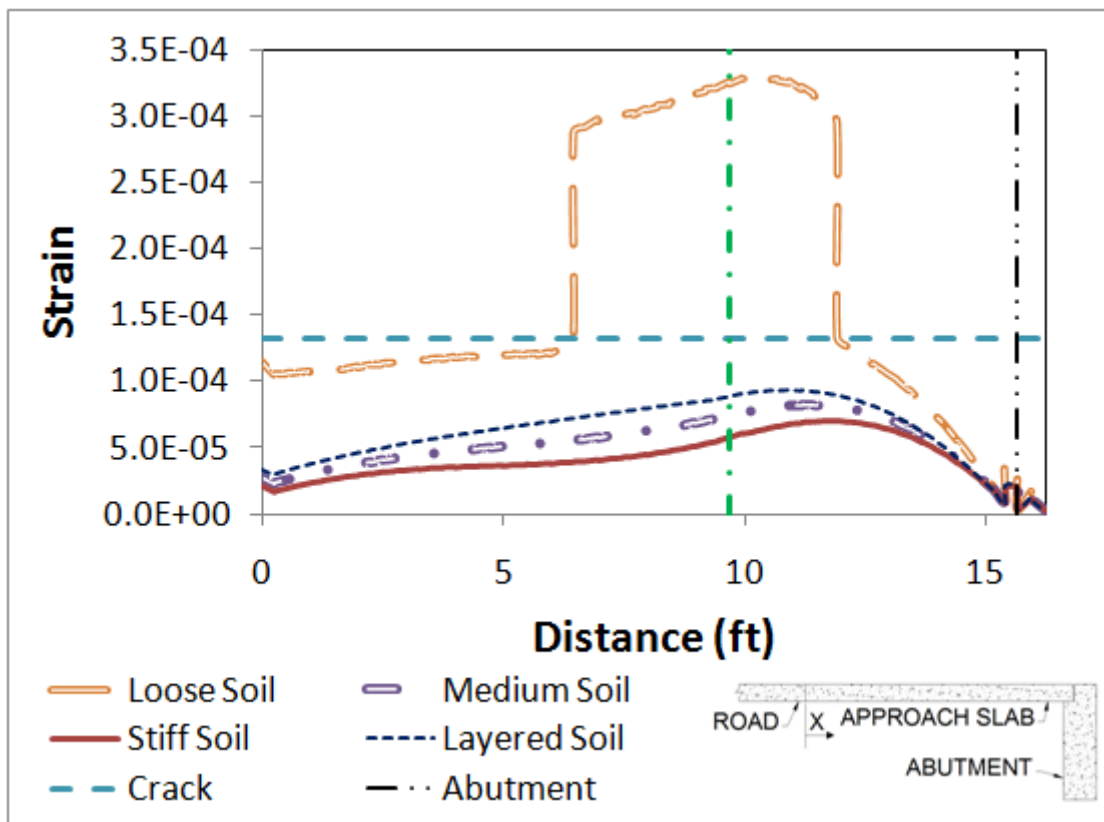
Figure 4.5 – Maximum principle (tensile) strain envelope for soil parametric study.

The joint rotations for each case analyzed were determined from the nodal displacement of the approach slab. Figure 4.6 displays the maximum calculated values of approach slab end rotation.
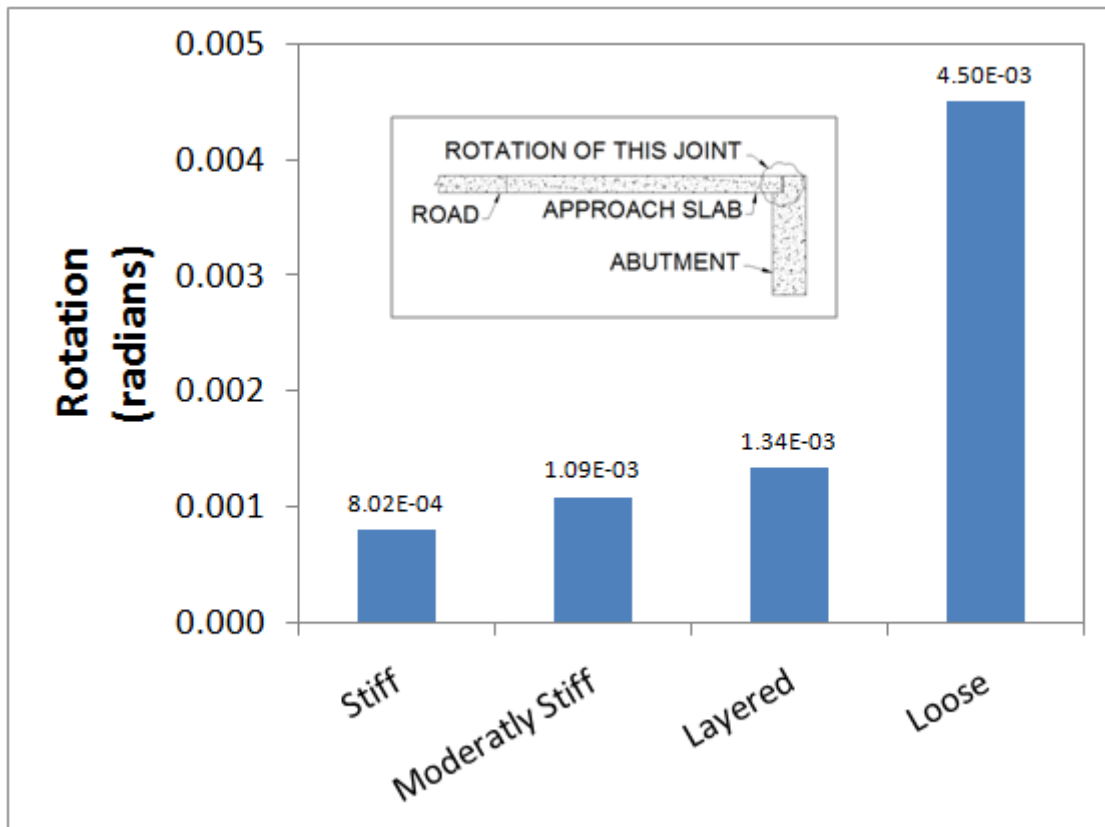
Figure 4.6 – Joint rotation for soil parametric study.

Settlement Trench and Abutment Geometry: Three abutment heights were included to determine their impact on the approach slab. Five settlement trench geometries were analyzed for each abutment height. Special consideration was taken to ensure the boundary condition on the lower region of the soil did not interfere with the soil behavior. To minimize any adverse effects on the model from the lower boundary condition, the depth of the soil beneath the bottom of the abutment was maintained constant. The depth of the influenced soil under the abutment was checked to ensure minimal adverse affects from the boundary condition. Figure 4.7 displays the maximum principle strains from the extreme bottom fiber of the approach slab for the 6' high abutment. The maximum principle strain and corresponding location for each case analyzed with the 6' abutment is presented in Tables 4.5 and 4.6.

Table 4.5 – Maximum principle (tensile) strains with location for 6' abutment study.

Case	Strain	Location
8' Trench	9.87E-05	10'-8 1/4"
6' Trench	8.23E-05	11'-2 1/4"
4' Trench	7.03E-05	11'-8 1/4"
2' Trench	6.82E-05	11'-8 1/4
No Trench	6.84E-05	11'-5 1/4"

Table 4.6 – Minimum principle (compressive) strains with location for 6' abutment study.

Case	Strain	Location
8' Trench	-1.06E-04	11'-3"
6' Trench	-9.04E-05	11'-9"
4' Trench	-7.92E-05	11'-9"
2' Trench	-7.70E-05	11'-9"
No Trench	-7.71E-05	11'-9"
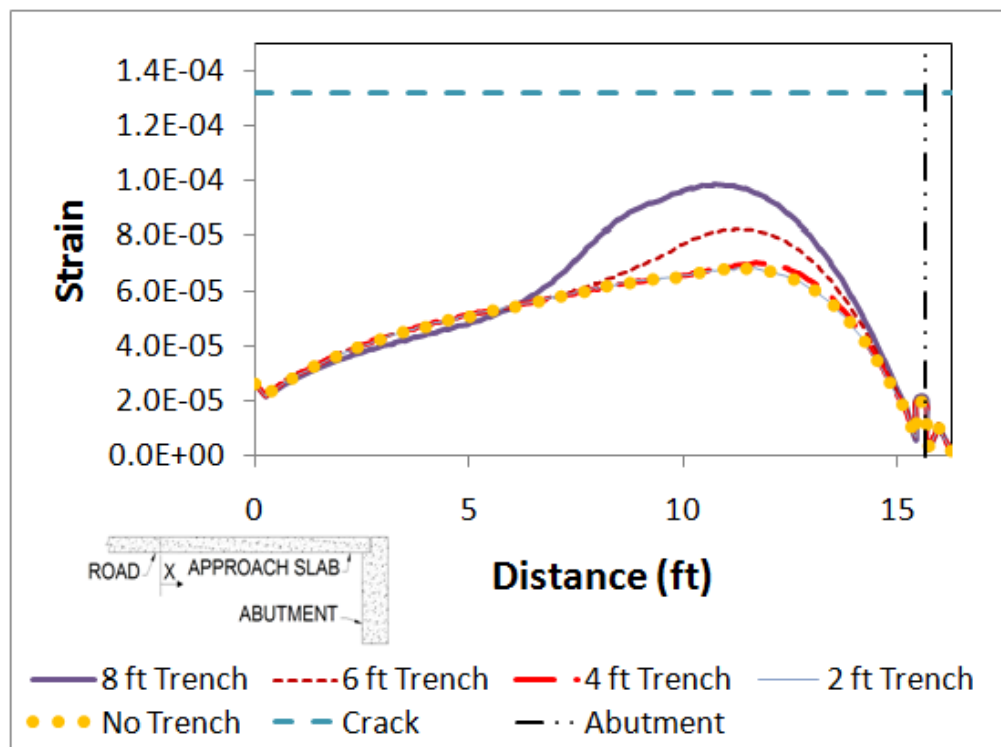
Figure 4.7 – Maximum principle strain of approach slab with a 6' high abutment.

Figure 4.8 displays the maximum principle strains from the extreme bottom fiber of the approach slab for the 8' high abutment. Tables 4.7 and 4.8 display the maximum principle strain and corresponding location for each case analyzed with the 8' abutment.

Table 4.7 – Maximum principle (tensile) strains with location for 8' abutment study.

Case	Strain	Location
8' Trench	1.03E-04	10'-11 1/4"
6' Trench	8.72E-05	11'-2 1/4"
4' Trench	7.64E-05	10'-11 1/4"
2' Trench	7.65E-05	10'-11 1/4"
No Trench	7.67E-05	10'-11 1/4"

Table 4.8 – Minimum principle (compressive) strains with location for 8' abutment study.

| Case	Strain	Location
8' Trench	-1.11E-04	11'-3"
6' Trench	-9.59E-05	11'-0"
4' Trench	-8.44E-05	11'-9"
2' Trench	-8.43E-05	10'-9"
No Trench	-8.45E-05	10'-9"
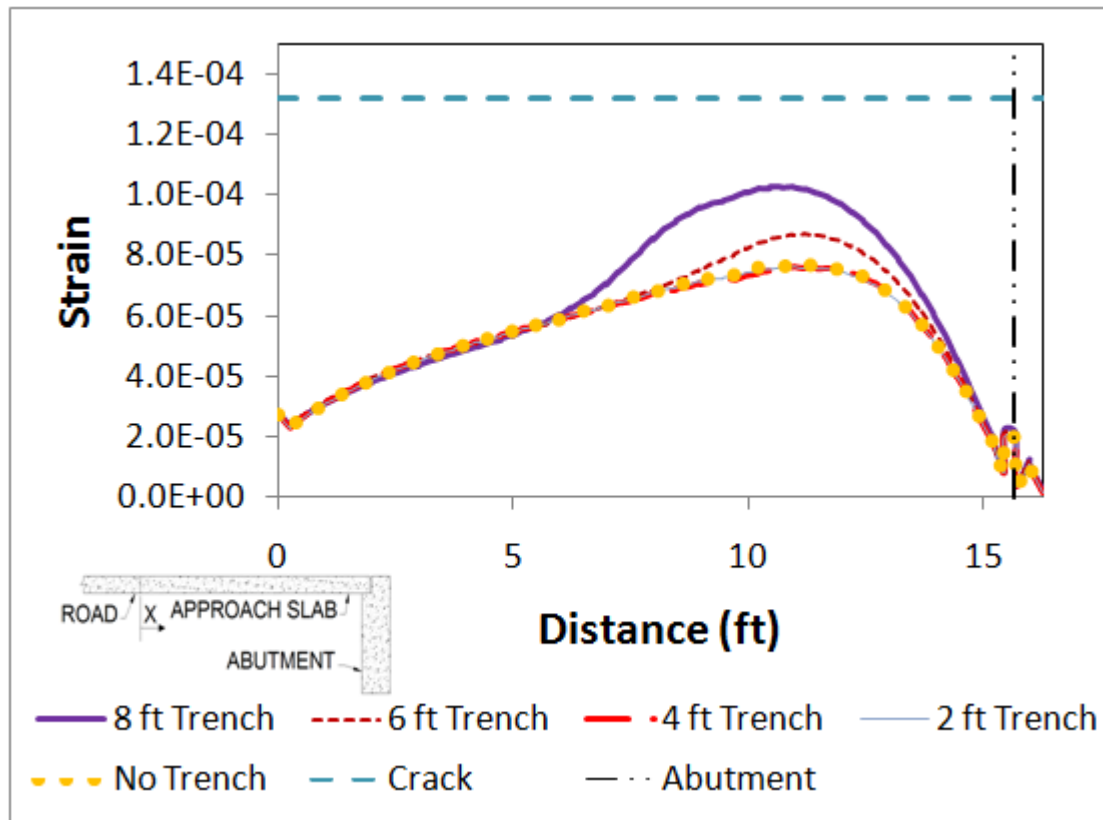
Figure 4.8 – Maximum principle strain of approach slab with a 8' high abutment.

Figure 4.9 displays the maximum principle strains from the extreme bottom fiber of the approach slab for the 12' high abutment. The maximum principle strain and corresponding location for each case analyzed with the 12' abutment is presented in Tables 4.9 and 4.10.

Table 4.9 – Maximum principle (tensile) strains with location for 12' abutment study.

Case	Strain	Location
8' Trench	1.11E-04	10'-5 1/4"
6' Trench	9.73E-05	10'-11 1/4"
4' Trench	9.32E-05	10'-11 1/4"
2' Trench	9.49E-05	10'-11 1/4"
No Trench	9.54E-05	10'-11 1/4"

Table 4.10 – Minimum principle (compressive) strains with location for 12' abutment study.

Case	Strain	Location
8' Trench	-1.17E-04	10'-6"
6' Trench	-1.02E-04	10'-9"
4' Trench	-9.92E-05	10'-9"
2' Trench	-1.01E-04	10'-9"
No Trench	-1.01E-04	10'-9"
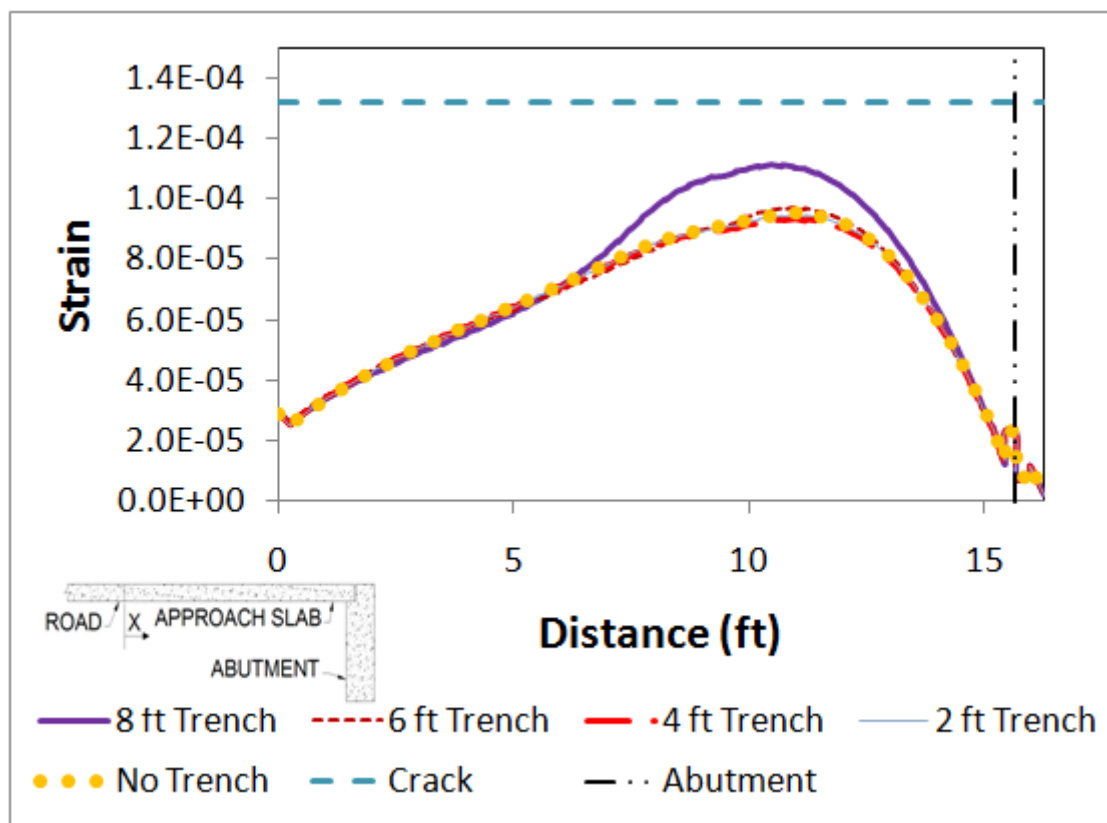
Figure 4.9 – Maximum principle strain of approach slab with a 12' high abutment.

Figure 4.10 displays the end rotation of the approach slab at the approach slab – abutment interface.
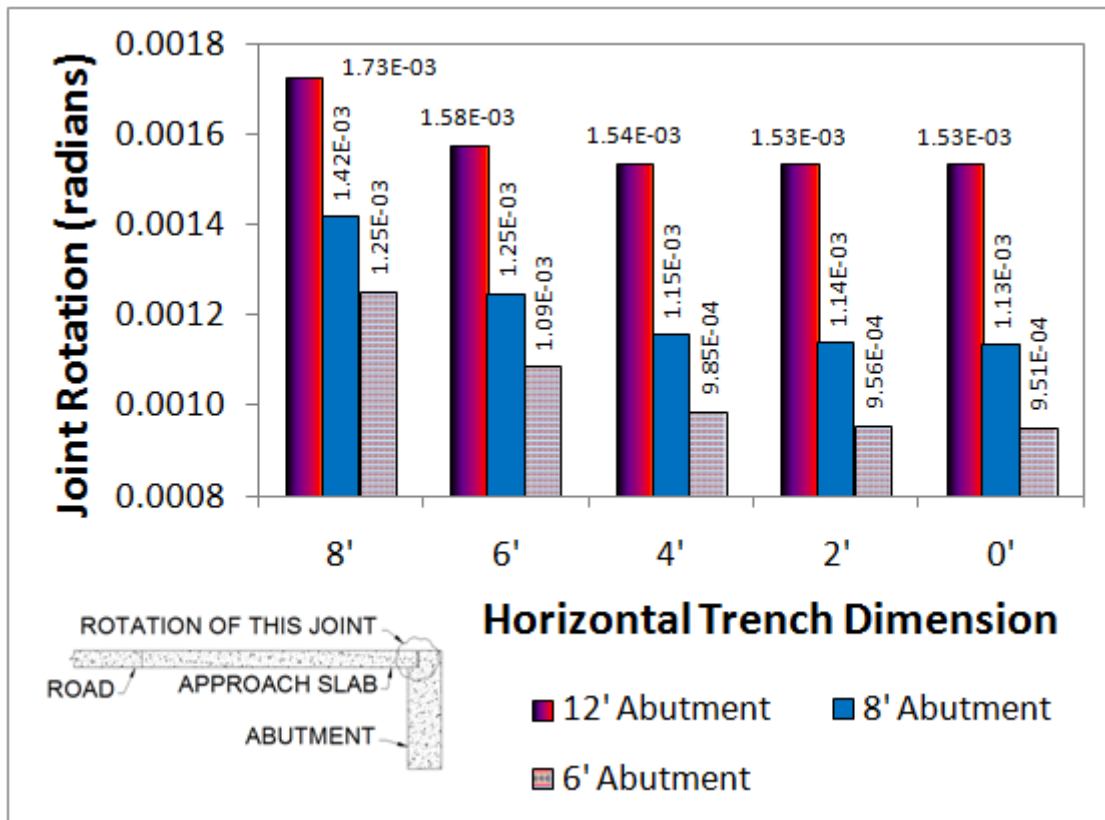
Figure 4.10 – Joint rotations for abutment and settlement trench parametric study.

Approach Slab Length: The length of the approach slab was varied from the base model to determine how the length of the approach slab affects strain and end rotation of the approach slab near the abutment. Approach slab lengths of 10' and 20' were analyzed and compared to the 15'-8" long approach slab used in the baseline model. Tables 4.11 and 4.12 display the location and magnitude of the maximum principle compressive strain calculated in the approach slab for each case analyzed.

Table 4.11 – Maximum principle (tensile) strains with location.

Case	Strain	Location
20'	8.21E-05	15'-6"
15'-8"	8.23E-05	11'-2 1/4"
10'	7.67E-05	6'-0"

Table 4.12 – Minimum principle (compressive) strains with location.

Case	Strain	Location
20'	-9.15E-05	16'-0 3/4"
15'-8"	-9.04E-05	11'-9"
10'	-8.47E-05	6'-6 1/2"

Figure 4.11 shows the maximum principle (tensile) strains of the bottom fiber of each approach slab analyzed. Figure 4.12 displays the joint rotation of each approach slab.
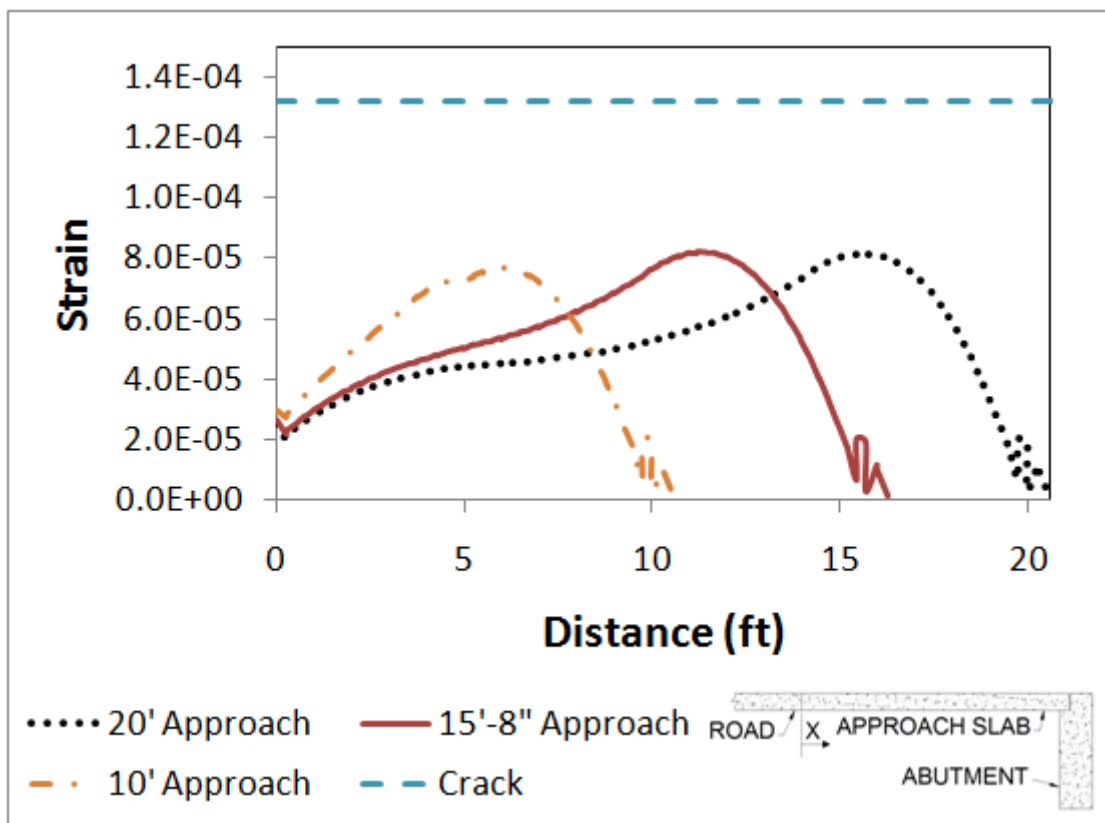
Figure 4.11 – Maximum principle strain of approach slabs with varying length.
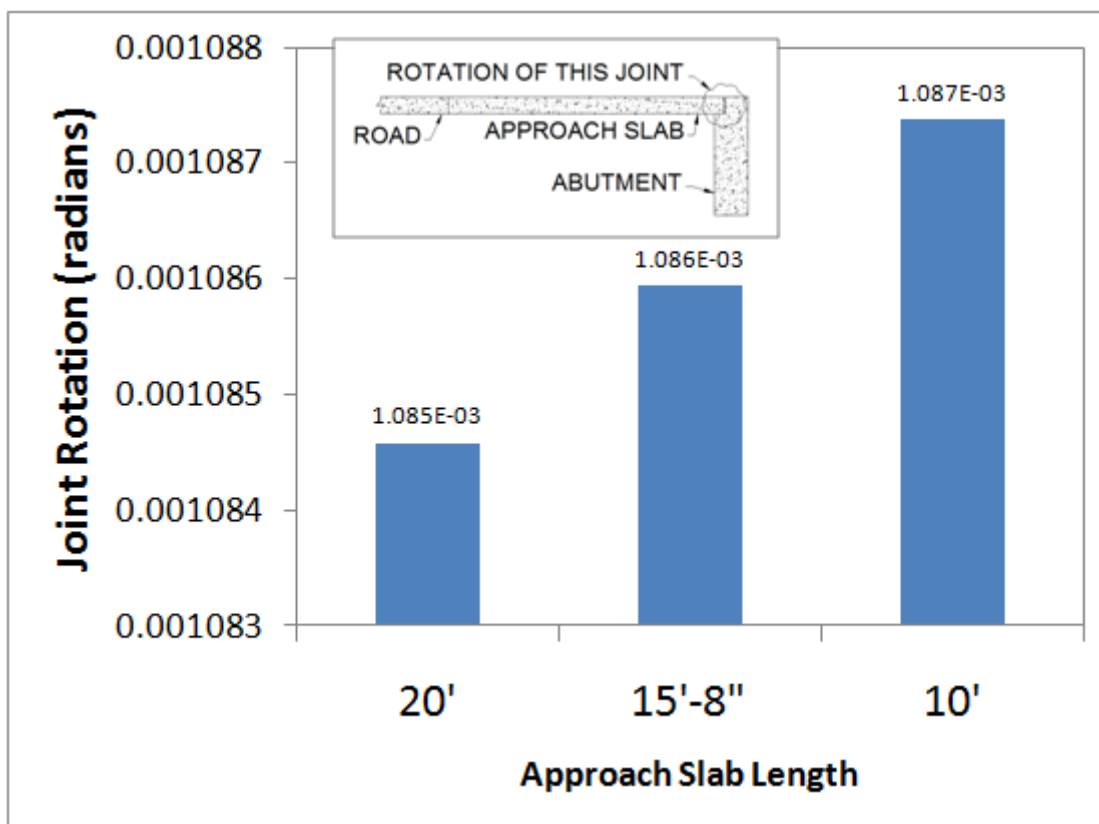
Figure 4.12 – Rotation of approach slab near the abutment for various approach slab lengths.

Concrete Stiffness: The initial 28 day concrete compressive strength (f_c') was based on a report submitted to the Wisconsin Highway Research Program (Naik, et al., 2006). The 28 day concrete compressive strength used in the baseline analyses was 4000 psi. An analysis was conducted to determine how an increase in the 28 day compressive strength would affect the approach slab. A 28 day compressive strength of 8000 psi was used in that comparison.

This parametric study investigated the cracking and joint rotation changes if a concrete with a higher compressive stress was utilized. The loose homogeneous soil profile was used for these analyses as this profile had exhibited tensile strains in the approach slab that exceeded the cracking strain. The largest maximum principle (tensile) strains were 0.000329 in/in at 10'-2 3/8" and 0.000104 in/in at 9'-2 3/8" for the 4 ksi and 8 ksi concrete, respectively. The largest minimum principle (compressive) strains were 0.000363 in/in at

10'-11 3/8" and 0.000109 in/in at 9'-0" for the 4 ksi and 8 ksi concrete, respectively. Figure 4.13 displays the maximum principle strains from the extreme bottom fiber of the approach slab for each analysis. The maximum end rotation of the approach slab near the abutment is presented in Figure 4.14.
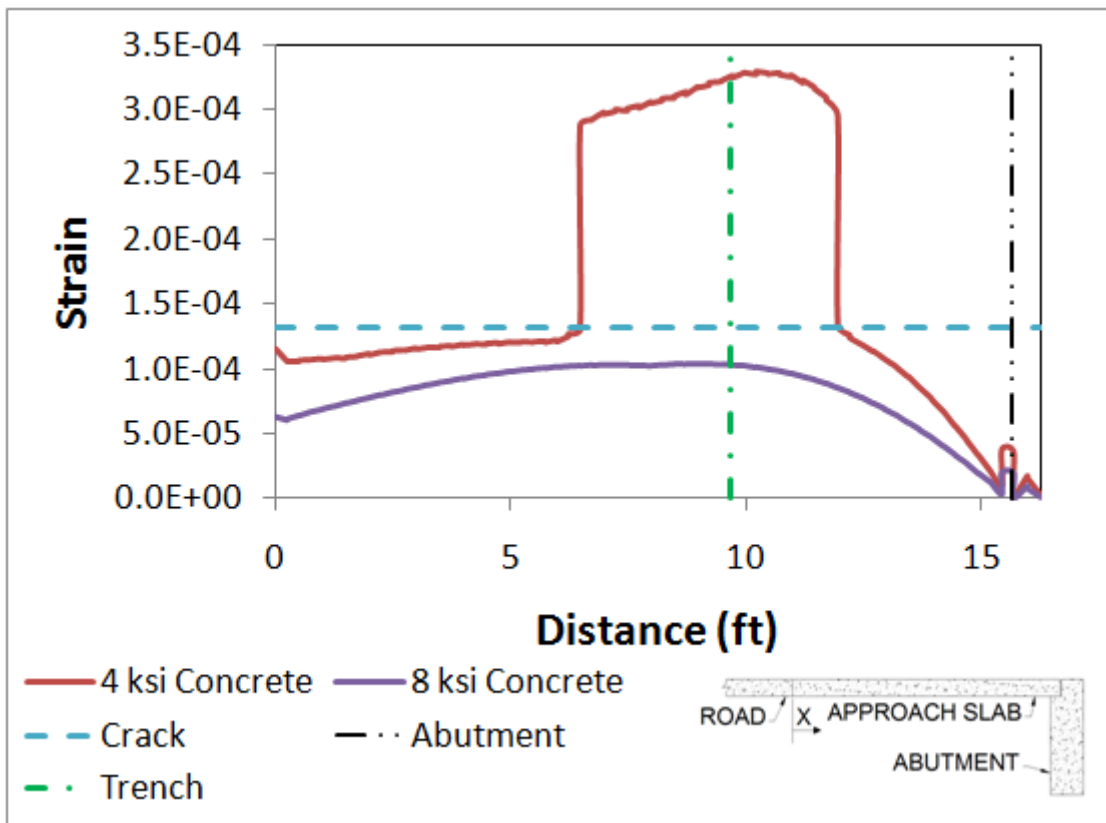
Figure 4.13 – Maximum principle strain of approach slabs with varying concrete stiffness.
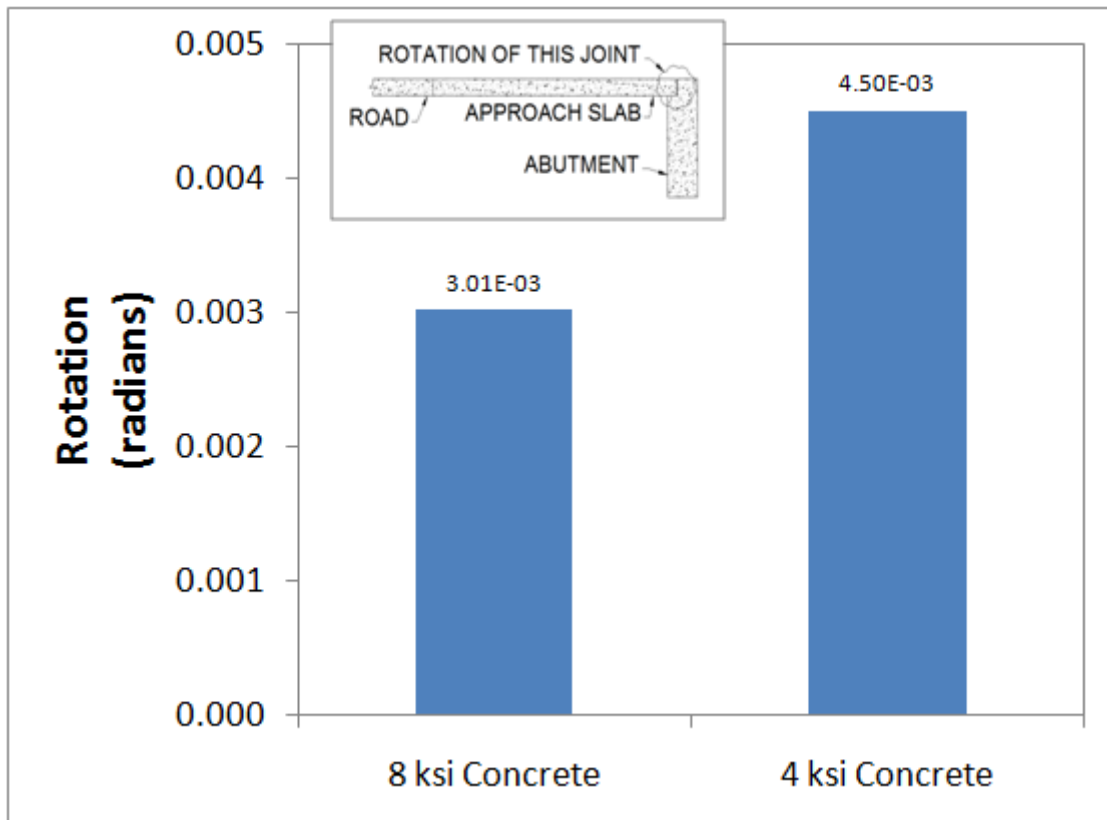
Figure 4.14 – Joint rotation for concrete stiffness parametric study.

Joint Restrictions: The constraint placed on the approach slab at the joint between the roadway and the approach slab was investigated to determine its impact on approach slab behavior. The couplings that were considered in this parametric study were:

- Shear Coupling
    - Horizontal and vertical displacement of one member was restrained relative to the other member.

- Moment Coupling
    - Both members were fixed to each other.

- No Coupling
    - Friction alone controlled the surface-to-surface contact.

The control point of the coupling constraint and location of the joint is shown in Figure 4.15.
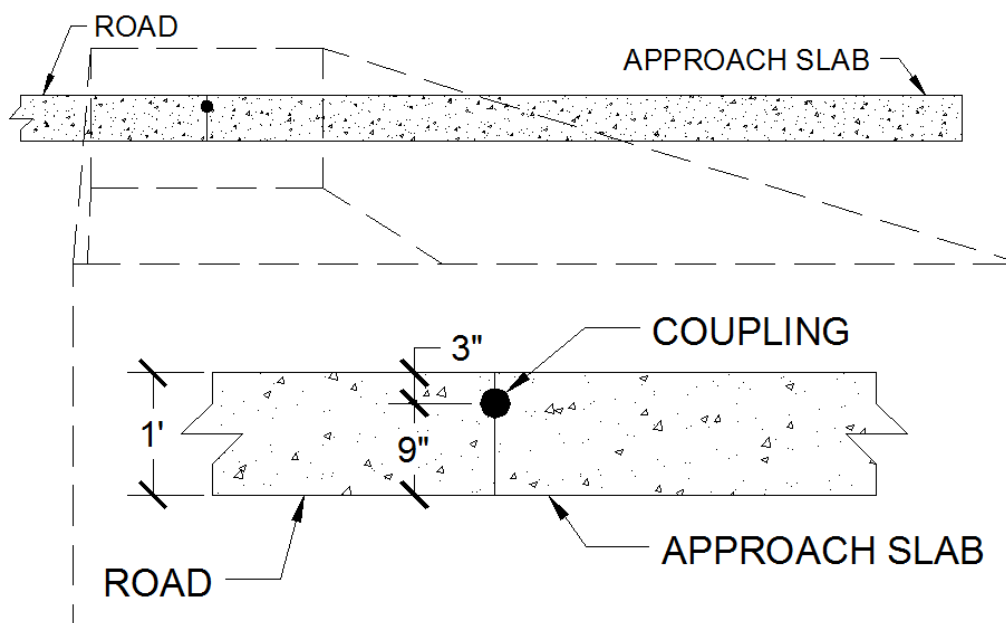
Figure 4.15 – Location of roadway – approach slab coupling.

The largest maximum principle (tensile) strain in the approach slab was 0.0000823 in/in at 11'-2 ¼", 0.0000823 in/in at 11'-2 ¼", and 0.0000807 in/in at 11'-2 ¼" for the moment, shear, and no coupling cases, respectively. The largest minimum principle (compressive) strain in the approach slab was 0.0000904 in/in at 11'-9", 0.0000904 in/in at 11'-9", and 0.0000895 in/in at 12'-0" for the moment, shear, and no coupling cases, respectively. Figure 4.16 displays the maximum principle (tensile) strain along the bottom of the approach slab for each joint restraint. Figure 4.17 displays maximum rotational displacements of the joint between the approach slab and abutment for the three parametric studies. The rotation of the end of the approach slab near the roadway was also determined for each case. Figure 4.18 displays this end rotation determined from each analysis.
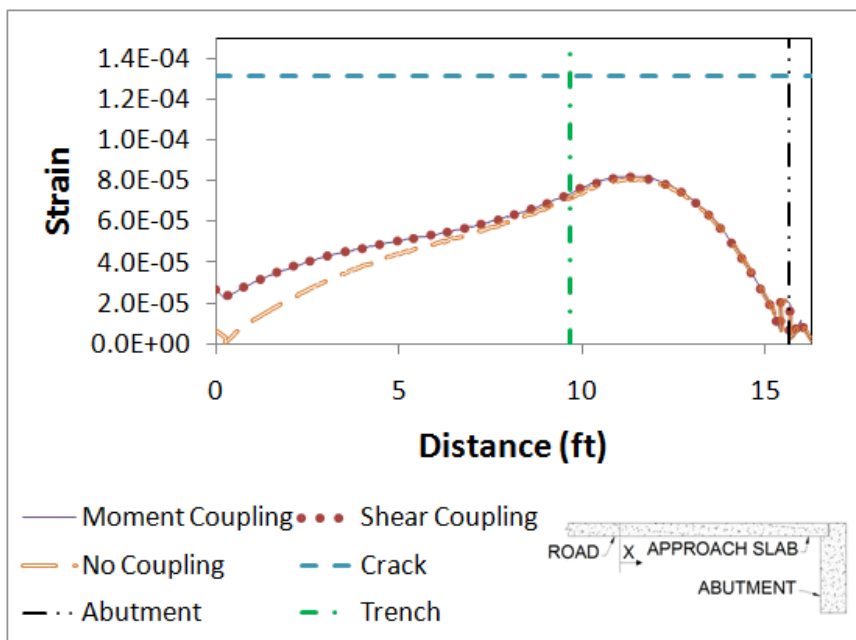
Figure 4.16 – Maximum principle (tensile) strains of approach slab for joint restriction study.
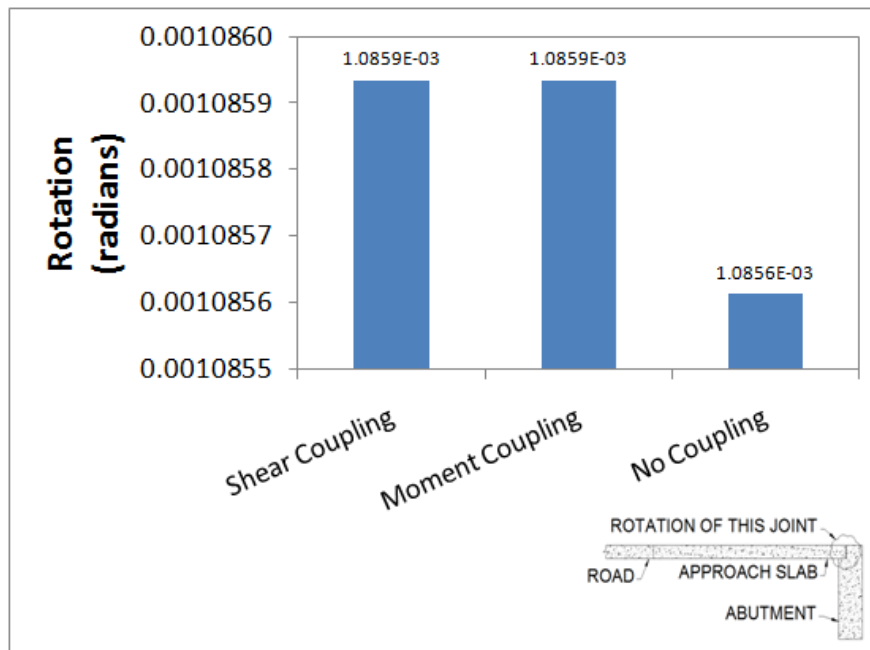
Figure 4.17 – Joint rotations for roadway – approach slab coupling study.
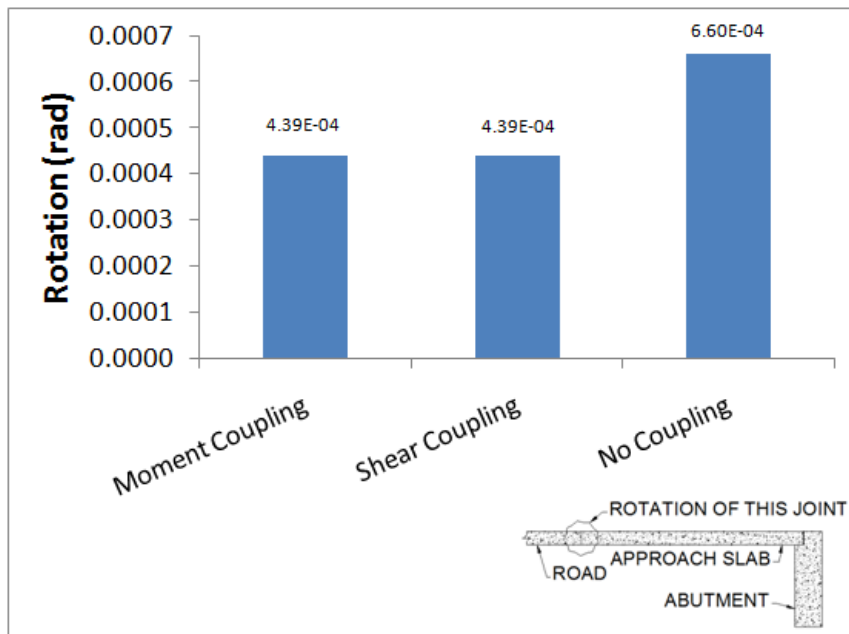
Figure 4.18 – Approach slab end rotation at the roadway-approach slab interface.

5. Discussion of Results

Introduction

Results from the analyses performed on the baseline model and subsequent parametric studies were examined to identify how the design variables affected the behavior of the approach slab. The end rotation of the approach slab at the approach slab-abutment interface and concrete cracking were the primary focus of the comparison. A pseudo load factor, the multiplier on service loads needed to cause cracking, was also defined. The geometry and material properties used in the baseline model best portrayed the median conditions that may exist at an actual bridge and are a focus of this examination. Each analysis was compared to the baseline model to determine the impact of that variable on the behavior of the approach slab.

## Assumptions with the Model

The concrete portions of the model utilized elastic properties alone. It was assumed that the moment of inertia was reduced by 33% for the entire region that had exceeded the cracking strain. This method yielded conservative results (assigning a lower stiffness to the cracked approach slab) as the entire region would not crack in a realistic slab. Discreet cracks would form with low stiffness.

The piles were assumed to be rigid for all analyses. This assumption was due to the large variety of geometry and materials used for piles. Actual pile stiffness and deflection was considered to be outside of the scope of this paper. The pile-abutment connection was also assumed to act as a rigid connection.

The expansion joint placed between the approach slab and abutment was assumed to have little resistance to expansion and contraction. The expansion joint between the approach slab and abutment was modeled as a 1" gap. This gap allowed the end of the approach slab to rotate without restraint.

Coupling between the roadway and approach slab simulated dowel bars embedded within the concrete to connect the parts together. It was assumed that the dowel bars would be placed at the quarter point and would have perfect bond and could resist pullout forces.

Pseudo Load Factor

Pseudo load factors were calculated for each analysis using the actual axle loads and spacing of the AASHTO HL93 tandem truck alone. These pseudo load factors were considered to be the factor that the service load needed to be increased for approach slab cracking to occur. This factor was not calculated for cases that exhibited approach slab cracking.

The pseudo load factor was determined by multiplying the largest maximum principle (tensile) strain observed in the approach slab by a factor that would result in cracking. This factor was used as the pseudo load factor for the corresponding analysis case.

Baseline Model Behavior

The strain computed from the numerical analysis did not result in approach slab cracking. The largest maximum principle (tensile) strain determined from the numerical analysis was 0.0000823 in/in at a distance of 11'-2 ¼" from the left edge of the approach slab. This strain was below the cracking strain of 0.000132 in/in.

The strains at the bottom and top of the approach slab were not equal and opposite for the baseline model. This is due to the presence of axial force created from the frictional restraint between the approach slab and abutment. The axial force shifted the location of the neutral axis down approximately 0.16 inches at the location of the largest maximum and minimum strains. The axial stress was calculated to be approximately 5 psi. The small magnitude of axial stress was ignored for all subsequent analyses

A load factor that would be required to crack the approach slab was calculated using the method and assumptions outlined previously. The load factor required for cracking in the base model was 1.60.

Base Model with Lane Loading

The model consisting of the lane loading alone was combined with the base model by superposition. Superposition was deemed acceptable because of the following reasons:

- The lane load and base model used the exact same geometry,
- Linear elastic properties were used to define all concrete parts used within the model,
- Equal plastic deformation of the soil was observed during the application of gravity for each model, and
- Plastic deformations produced in the baseline model were observed at two elements near the start of the settlement trench. These deformations were considered negligible.

The largest maximum principle (tensile) strain in the approach slab was 0.000118 in/in, less than the cracking strain, measured at a distance of 11'-2 ¼" from datum after superposition had been applied to the two models.

A cracking load factor was determined for the baseline model with lane loading. The factor that would be required for cracking to occur would be 1.11. Since this is less than the AASHTO impact factor, the actual loads on the approach slab would exceed the cracking load and result in approach slab deterioration. The change in the impact factor (1.60 to 1.11) shows that the lane load has a significant effect on the strain of the approach slab when coupled with the tandem vehicle.

Superposition was also used to determine a maximum end rotation of 0.00189 radians at the abutment joint.

Parametric Study Discussion

Settlement Trench

The geometry of the settlement trench was varied from the baseline model to determine how a settlement trench influenced the behavior of the approach slab. Three additional settlement trench geometries (and no trench) were analyzed modifying the geometry of the baseline model. Figure 3.41 displays the geometry of each settlement trench considered in this study.

Results from the settlement trench parametric study suggest the behavior of an approach slab is significantly affected when the settlement trench is larger than 4ft. A 2.7% difference in the largest maximum principle tensile strain was observed between the approach slab with a 4ft. settlement trench and the case without a settlement trench. The difference increased to 15.7% when the 4ft. settlement trench was compared to the 6ft. settlement trench. A difference in strain of 18.1% was observed between the 6 and 8 ft. settlement trenches.

The rotations at the end of the approach slab had a maximum 3.52% difference between the 4ft. settlement trench and no trench, a 9.79% difference between the 6 and 4ft. settlement trenches, and a 14.3% difference between the 6 and 8ft. settlement trenches.

In general, it did not appear that a settlement trench affected strains in the approach slab significantly until the trench became longer than 4feet. End rotations at the abutment joint were not increased significantly by the trench until the trench length reached 6 foot or greater.

The pseudo load factor needed to cause cracking for each case analyzed is shown in Table 5.1. The factor calculated for the 8ft. settlement trench is equal to the impact factor recommended by AASHTO. It is logical to assume that the presence of the lane load with the tandem would reduce the pseudo load factor or would have caused cracking of the approach slab.

Table 5.1 – Load factor for settlement trench study (tandem only).

Trench	Impact Factor 6' Abutment
8' Trench	1.33
6' Trench	1.60
4' Trench	1.89
2' Trench	1.93
No Trench	1.93

Abutment Height

The abutment height parametric study considered the abutment height used in the baseline model as well as two additional heights. A total of four different settlement trench geometries were analyzed with each abutment height for a combined parameter analysis.

The baseline model used a 6 foot abutment height. The other abutment heights that was considered in the parametric study were 8ft and 12ft..

Changing the abutment height had little effect on the approach slab strain or cracking except when a settlement trench length greater than 6ft was present. Then the change in abutment height from 6ft to 12ft caused a strain increase of only 12%.

Abutment height did have some effect on the slab end rotation. Changing the height from 6ft to 12ft increased the rotation by 38% with an 8ft trench and 61% with no trench.

Pseudo Load Factor for Abutment Height Study: The load factors to cause cracking for each case analyzed with varying abutment height is shown in Table 5.2. The factor calculated for the 8ft. settlement trench cases is less than or equal to the impact factor recommended by AASHTO and those slabs would be expected to readily show cracking. It is logical to assume that the presence of the lane load would reduce the load factor or would have caused more cracking of the approach slab.

Table 5.2 – Load factor for settlement trench study.

Trench	Impact Factor		
	6' Abutment	8' Abutment	12' Abutment
8' Trench	1.33	1.28	1.18
6' Trench	1.60	1.52	1.36
4' Trench	1.89	1.74	1.42
2' Trench	1.93	1.74	1.38
No Trench	1.93	1.74	1.37

Approach Slab Length

Cracking was not observed for any of the approach slab lengths analyzed when on moderately stiff soil. All of the cases used the same trench geometry that was used in the baseline model.

The maximum strain computed in the 20' and 15'-8" approach slab length cases exhibited little variation between each other while the 10' approach slab showed lower strains. The maximum difference in tensile strains was only 8% between the different slab lengths. There was virtually no change in slab end rotations with the different lengths.

Load Factor for Approach Slab Length Study: The load factors to cause cracking for the approach slab length parametric study were determined. The factors are presented in Table 5.3. Again the small influence of slab length on the load factor is apparent.

Table 5.3 – Load factors for approach slab parametric study.

Length	Factor
20'	1.60
15'-8"	1.60
10'	1.73

Soil Stiffness

The soil stiffness parametric study investigated the influence the soil had on approach slab strains and rotations. Four analyses were performed in this parametric study. The soil stiffness parametric studies performed were intended to represent the upper, lower, and typical soil properties that may be present under an approach slab. Loose and stiff soil properties encompassed the lower and upper bounds of the soil stiffness while the moderately stiff soil represented the typical soil properties. The layered soil analysis case represented increases in effective stress with depth.

Cracking was predicted in the loose soil analysis (strain was larger than the cracking strain of 0.000132) but not for either of the other soils.

Analysis results show a decrease in strain with soil stiffness increase. The tensile strain difference between the stiff and moderately stiff soil was 15.2%. A 12.9% difference was observed between the layered and moderately stiff case. There were only these little variations between the results with the stiff, moderate or layered soil. The loose soil, however, had tensile strains that were 460% of the stiff soil values.

Slab end rotations varied by 67% between the stiff and layered soils. In the loose soil the rotations increased by 460% compared to the stiff soil. Clearly the soil type can have a significant impact on the slab performance when the soil stiffness becomes very low.

Load Factor for Soil Stiffness Study: The load factor to cause cracking of the slab for each soil analyzed in the soil stiffness parametric study was determined from the strain information collected from each analysis. Table 5.4 displays the load factor for each soil. The load factor for the loose soil is not applicable as the approach slab had cracked from the truck load alone.

Table 5.4 – Load factors for soil stiffness parametric study.

Case	Factor
Stiff Soil	1.85
Moderately Stiff	1.60
Layered Soil	1.40
Loose Soil	NA

Concrete Stiffness

Two concrete stiffness parameters were investigated. The largest maximum principle (tensile) strains calculated in the numerical analysis were 0.000329 in/in and 0.000104 in/in for the 4 ksi and 8 ksi concrete, respectively. The change represented a 216% increase in strain for the 4ksi slab. On the loose soil the 4 ksi concrete exhibited cracking while the 8 ksi concrete did not crack. The end rotation were 50% higher with the low strength slab.

It appears from these results that using higher strength concrete, such as available with precast concrete, would clearly be wise if poor soil conditions are present.

Load Factor for Concrete Stiffness Study: The load increase factor to cause slab cracking was calculated for the 8 ksi concrete only, as the 4 ksi concrete cracked under the service truck load alone when on loose soil. The calculated load factor was 1.28 for the 8 ksi concrete without the lane load.

Joint Restrictions

Constraints placed on the coupling between the roadway and approach slab were varied to determine the impact this restraint had on the behavior of the approach slab. Two constraints were considered in addition to the baseline model. The restraints utilized a moment and shear coupling or an unrestrained coupling placed between the roadway and approach slab. The largest maximum principle (tensile) strain determined from the analysis was 0.0000807 in/in for the unrestrained coupling case and 0.0000823 in/in for both the moment and shear couplings.

The unrestrained analysis was performed to investigate the behavior of the approach slab if the expansion joint would be relocated to the joint between the roadway and approach slab rather than at the abutment. The largest maximum principle (tensile) strain for the unrestrained case was 0.0000807 in/in at a location of 11'-2 ¼" from datum.

The strain computed from the unrestrained case exceeded each restrained case. This is due to excessive movement of the approach slab at the joint between the roadway and approach slab. The absence of any coupling would allow differential movement of each part at the joint location. This differential movement created a 'bump' at the joint between the roadway and approach slab as the truck traversed the approach slab. The maximum end rotation of the approach slab at this joint was 0.000440 radians for both the moment and shear coupling and 0.000660 radians for the unrestrained case.

6. Summary and Conclusions

Summary

Abutment and Settlement Trench Geometry: A settlement trench only affected the approach slab response significantly when the trench had a length of 6ft or greater. Settlement trenches less than or equal to 4' had a small impact on the behavior of the approach slab for the abutment heights considered. The degree to which the larger settlement trenches influenced the approach slab strains was dependent on the height of the abutment with a change in slab end rotation of 12% between a 6ft and 12ft high abutment.

Abutment height influenced the behavior of the approach slab for all cases analyzed. Strains computed in the approach slab were consistently higher (34%) for taller abutments. End rotation of the approach slab was influenced in the same way as the strain. The end rotation for a 12ft high abutment with an 8ft trench was 0.00173 radians while a 6ft abutment with no trench had an end rotation of 0.00125 radians.

Approach Slab Length: The length of the approach slab only had a small influence on the behavior of the approach slab as measured by slab strains. There was virtually no impact on the measured slab end rotation.

Soil Stiffness: The soil stiffness had little effect on either slab strains or end rotations for the stiff, moderate and layered soils. Loose soil, however, can have a major impact on the slab behavior. Between the stiff soil and loose soil the slab strains increased by 360% and the end rotation increased by 460%. The loose soil was the only soil condition that caused cracking of the approach slab under truck loading. The cracking, and loss of stiffness, created the large end rotations.

Concrete Stiffness: The effect of concrete stiffness was only examined with a loose soil condition. Concrete cracking was observed with the lower stiffness (4ksi strength) approach slab but was prevented when the concrete stiffness (8ksi strength) was increased. This implies that a precast approach slab with higher concrete strength would inherently

exhibit less cracking than a cast in place slab with lower strength. End rotation of the approach slab was increased by 50% with the decrease in concrete strength and stiffness.

End Rotation: The range of end rotations developed by the approach slab near the abutment was significant. The rotation was consistently under 0.002 radians for all but the loose soil analysis. The maximum rotation observed was 0.0045 radians with the low strength concrete (4 ksi) and loose soil.

Load Factor for Cracking: A load factor that would be needed to cause cracking in the approach slab was determined for each analysis that did not result in approach slab cracking from the HL93 tandem truck alone. The calculated load factor for those conditions ranged from 1.93 to 1.18 with a median factor of 1.60.

Conclusions

Approach Slab End Rotation: The end rotation of the approach slab near the abutment varied depending on geometry of the approach slab, trench and abutment as well as with the stiffness of the soil and concrete used in the analyses. A maximum rotation of 0.0045 radians was computed from the analyses in a situation with a loose soil and 4 ksi concrete slab. The majority of the rotations in other cases were below 0.002 radians. For normal soil conditions the expansion joint or ductile concrete between the approach slab and abutment should be design to accommodate a minimum of 0.002 radians of rotation.

Approach Slab Cracking: The susceptibility of the approach slab to cracking was influenced by the height of the abutment, trench length, slab length, soil stiffness, and concrete stiffness. The following conclusions were made concerning the previously mentioned variables.

Taller abutments increase the likelihood of concrete cracking in the approach slab. This was particularly true for all settlement trenches with length less than 6ft. When the settlement trench was 6ft or more in length the slab was not particularly sensitive to abutment height.

The length of the approach slab has little effect on the likelihood of cracking or amount of end rotation for slabs greater than 10ft in length.

Stiff soil under the approach slab reduced the probability of concrete cracking. The risk of concrete cracking increased as the soil stiffness decreased. With loose soil, slab cracking can be expected with normal strength (4ksi) concrete. Cracking was less likely when a concrete with a higher compressive stress was used for the approach slab (i.e. 8ksi vs. 4ksi).

7. References

AASHTO, LRFD specification for Highway Bridge Design, American Association of Highway and Transportation Officials, 5th Ed., 2010

ACI, ACI 318 Standard Specifications for Design of Concrete Building Structures, American Concrete Institute, Committee 318, 2008

Cook Robert D [et al.] Concepts and Applications of Finite Element Analysis [Book]. - [s.l.] : John Wiley & Sons, Inc., 2002. - Vol. IV.

Cosgrove Edward F and Lehane Barry M Cyclic Loading of Loose Backfill Placed Adjacent to Integral Bridge Abutments [Report]. - [s.l.] : International Journal of Physical Modelling in Geotechnics 3, 2003.

CTC & Associates, LLC Concrete Bridge Approach Pavements: A Survey of State Practices [Report]. - Madison : WisDOT Research & Library Unit, 2010.

Edil T. B., Benson C. H. and Bareither C. A. Determination of Shear Strength Values for Granular Backfill Material Used by the Wisconsin Department of Transportation, Report SPR # 0092-05-08 [Report]. - 2007.

FHWA Continuously Reinforced Concrete Pavement [Online] // Federal Highway Administration Pavements Technical Advisory. - U.S. Department of Transportation, June 5, 1990. - October 20, 2010. - http://www.fhwa.dot.gov/pavement/t508014.cfm.

Fredlund D.G and Rahardjo H. Soil Mechanics for Unsaturated Soils [Book]. - [s.l.] : John Wiley & Sons, Inc., 1993.

Gere James M Mechanics of Materials [Book]. - [s.l.] : Brooks/Cole, 2004. - Vol. 6th Edition.

Ha Hunsoo, Seo Jeong Bok and Briaud Jean-Louis Investigation of Settlement at Bridge Approach Slab Expansion Joint: Numerical Simulations and Model Tests [Report]. - College Station : Texas A&M University, 2002.

Hall Kevin D and James Mainey PCC Inputs to Mechanistic-Empirical Pavement Design Guide [Report]. - 2008.

Helwany Sam Applied Soil Mechanics with ABAQUS Applications [Book]. - [s.l.] : John Wiley & Sons, Inc., 2007.

Helwany Sam, Koutnik Therese Ellen and Ghorbanpoor Al Evaluation of Bridge Approach Settlement Mitigation Methods [Report]. - Milwaukee : University of Wisconsin, 2007.

Hoppe Edward J Guidelines for the Use, Design, and Construction of Bridge Approach Slabs [Report]. - Charlottesville : Virginia Department of Transportation, 1999.

Jardine R. J., Lehane B. M. and Everton S. J. Friction Coefficients for Pile in Sands and Silts [Report]. - [s.l.] : Society for Underwater Technology, 1993.

Merritt David K [et al.] Construction of the Iowa Highway 60 Precast Prestressed Concrete Pavement Bridge Approach Slab Demonstration Project [Report]. - Austin : The Transtec Group, Inc., 2007.

Naik Tarun R., Chun Yoon-Moon and Kraus Rudolph N. Investigation of Concrete Properties to Support Implementation of the New AASHTO Pavement Deisgn Guide [Report]. - Milwaukee : University of Wisconsin, 2006.

Puppala Anand J [et al.] Recommendations for Design, Construction, and Maintenance of Bridge Approach Slabs: Synthesis Report [Report]. - [s.l.] : FHWA, 2008.

Schuettpelz C.C., Fratta D. and Edil T.B. Mechanistic Corrections for Determining the Resilient Modulus of Base Course Materials Based on Elastic Wave Measurements [Report]. - [s.l.] : ASCE Journal of Geotechnical and Geoenvironmental Engineering, 136(8):1086-1094, 2010.

Seo Jeong Bok The Bump at the End of the Bridge: An Investigation [Report]. - College Station : Texas A&M University, 2003.

Stark T. K., Olson S. M. and Long J. H. Differential Movement at the Embankment/Structure Interface - Mitigation and Rehibilitation Report No. IAB=H1 [Report]. - Springfield : Illinois Department of Transportation, 1995.

Wahls H. E. NCHRP Synthesis of Highway Practices 159: Design and Construction of Bridge Approaches. [Report]. - Washington D.C. : Tranportation Research Board, National Research Council, 1990.

White David J [et al.] Underlying Causes for Settlement of Bridge Approach Pavement Systems [Journal]. - [s.l.] : ASCE, 2007. - July/August.

Wisconsin Department of Transportation WisDOT Bridge Manual [Book]. - 2009.

Zaman M., Gopalasingam A. and Laguros Consolidation of Settlement of Bridge Approach Foundations [Journal]. - [s.l.] : Journal of Geotechnical Engineerings, ASCE, 1991. - Vol. 11.

CFIRE

University of Wisconsin-Madison
Department of Civil and Environmental Engineering
1410 Engineering Drive, Room 270
Madison, WI 53706
Phone: 608-263-3175
Fax: 608-263-2512
cfire.wistrans.org